Retinal input integration in excitatory and inhibitory neurons in the mouse superior colliculus *in vivo*

Carolin Gehr[1-4], Jérémie Sibille[1-4], Jens Kremkow[1-4]

[1]Neuroscience Research Center, Charité-Universitätsmedizin Berlin, Charitéplatz 1,10117 Berlin

[2]Bernstein Center for Computational Neuroscience Berlin, Philippstraße 13, 10115 Berlin

[3]Institute for Theoretical Biology, Humboldt-Universität zu Berlin, Philippstraße 13, 10115 Berlin

[4]Einstein Center for Neurosciences Berlin, Charitéplatz 1,10117 Berlin

Send correspondence to:
Jens Kremkow
Neuroscience Research Center
Charité - Universitätsmedizin Berlin
Charitéplatz 1
10117 Berlin, Germany
Phone: +49 30 450 639081
Email: jens.kremkow@charite.de
Web: kremkowlab.com, twitter.com/Kremkow

ABSTRACT

The superior colliculus (SC) is a midbrain structure that contains one of the highest densities of inhibitory neurons in the brain and, together with the thalamocortical visual system, it plays a key role in visually guided behaviors. The SC receives direct inputs from retinal ganglion cells (RGCs) but whether excitatory and inhibitory SC neurons differentially integrate retinal activity *in vivo* is still largely unknown. We recently established an extracellular recording approach using high-density electrodes to measure the activity of RGCs simultaneously with their postsynaptic SC targets *in vivo*, that allows addressing how SC neurons integrate RGC activity. Here, we employ this method to study the functional properties and dynamics that govern retinocollicular signaling in a cell-type specific manner by identifying GABAergic SC neurons using optotagging in anesthetized VGAT-ChR2 mice. We measured 305 monosynaptically connected RGC-SC pairs, out of which approximately one third of retinal afferents connect onto inhibitory SC neurons. We show that both excitatory and inhibitory SC neurons receive comparably strong RGC inputs, with functionally similar RGC-SC pairs showing stronger connections. Our results demonstrate that similar wiring rules apply for RGCs innervation of both excitatory and inhibitory SC neurons, which is unlike the cell-type specific connectivity in the thalamocortical system. Contrasting the similar RGC-SC connection strength, we observed that RGC activity contributed more to the activity of postsynaptic excitatory SC neurons than to the activity of postsynaptic inhibitory SC neurons. This implies that the excitatory SC neurons are more specifically coupled to RGC afferent inputs, while inhibitory SC neurons may integrate additional inputs from other sources. Taken together, our study deepens the understanding of cell-type specific retinocollicular functional connectivity and emphasizes that the two major brain areas for visual processing, the visual cortex and the superior colliculus, differently integrate sensory afferent inputs.

INTRODUCTION

The mouse superior colliculus (SC) is a midbrain structure that receives direct inputs from retinal ganglion cells (RGCs) (Drager and Hubel, 1976; Ellis et al., 2016; Huberman et al., 2008; Kremkow and Alonso, 2018). Together with the visual cortex (Glickfeld et al., 2013; Lashley, 1931; Niell and Scanziani, 2021; Petruno et al., 2013), the SC plays a key role in visually guided behaviors (Evans et al., 2018; Hoy et al., 2019; Shang et al., 2019, 2015; Wei et al., 2015). Intriguingly, the visual SC layers contain one of the highest densities of inhibitory (GABAergic) neurons in the brain (Kaneda et al., 2008; Ranney Mize, 1992) suggesting that inhibition plays a key role in visual processing within the SC. Indeed, inhibitory SC neurons (INs) are known to be involved in several sensory functions including surround suppression (Kasai and Isa, 2016) and motion processing (Barchini et al., 2018; Gale and Murphy, 2016), but also in the regulation of wakefulness (Zhang et al., 2019). However, how GABAergic SC neurons are recruited by their retinal inputs *in vivo* remains largely unknown (Shi et al., 2017). An understanding of how RGC inputs are integrated by SC INs and SC excitatory neurons (EXNs) is crucial for reaching a mechanistic understanding of the computations within the SC microcircuit.

In sensory systems, the divergence of long-range afferent axons onto GABAergic and non-GABAergic neurons ensures a balance between excitation and inhibition (E/I) (Miller, 2016). For example, in sensory cortices, thalamic afferents differentially activate excitatory and local inhibitory neurons (Cruikshank et al., 2007; Ji et al., 2016) with a stronger drive onto inhibitory neurons compared to excitatory neurons (Bruno and Simons, 2002; Cruikshank et al., 2007; Gabernet et al., 2005; Gibson et al., 1999; Inoue and Imoto, 2006; Swadlow, 2003). This stronger drive on inhibitory neurons establishes an effective feedforward inhibition (Agmon and Connors, 1992; Bereshpolova et al., 2020; Gabernet et al., 2005; Kremkow et al., 2010a, 2010b; Sun et al., 2006) that balances the excitation from thalamic afferents (Isaacson and Scanziani, 2011) and contributes to sharpening stimulus feature selectivity (Lee et al., 2012). Moreover, this wiring motif can partly be linked to the response properties of cortical inhibitory neurons as they typically show higher firing rates, broader tuning, low selectivity and high sensitivity (Alonso and Swadlow, 2005; Bruno and Simons, 2002; Gibson et al., 1999; Kremkow et al., 2016; Porter et al., 2001; Swadlow et al., 2002) to facilitate feedforward inhibition in response to thalamic input. Despite the importance of this afferent wiring motif for sensory processing in the thalamocortical visual circuit, it is currently unknown whether the retinocollicular pathway follows similar or different principles.

We recently demonstrated that SC neurons can receive strong input from RGC axons *in vivo* (Sibille et al., 2022a). Moreover, around one third of retinocollicular synapses connect onto inhibitory neurons that form intrinsic connections within the SC (Whyland et al., 2020). These findings support the notion that an effective feedforward inhibition might also be at play in the retinocollicular system.

But whether afferent inputs are differentially integrated by excitatory and inhibitory SC neurons, similar to the thalamocortical system, is unknown. However, our previous study in the retinocollicular system lacks the cell-type specificity, and it remains an open question whether the strong drive is specific to inhibitory SC neurons or if it is a general property of retinocollicular connections, and thus cell-type independent. Therefore, whether there are any differences in connection strengths between RGCs that project to excitatory and inhibitory SC neurons remains elusive. In this study, we investigate how excitatory and inhibitory neurons in the SC integrate retinal inputs *in vivo*.

We aim to answer these questions by characterizing the properties of the long-range synaptic connections between RGC-SC pairs employing a set of measurements: 1. The connection efficacy is used to study how strongly excitatory and inhibitory SC neurons are driven by their RGC input. 2. The functional similarity is analyzed between connected RGC-SC pairs to examine whether comparable wiring motifs govern retinocollicular signaling in excitatory and inhibitory neurons. 3. Short-term dynamics of retinal activity are studied to estimate whether the retinal spiking pattern shows paired-spike enhancement on retinocollicular synapses. Finally, 4. the connection contribution is employed to investigate how tightly the SC activity is coupled to retinal spiking.

This study intends to generate a more detailed picture of cell-type specific retinocollicular innervation and to fill a gap concerning the different long-range functional connectivity motifs that exist along the visual pathways.

RESULTS

Recording excitatory and inhibitory neurons simultaneously with RGC axons in the mouse SC *in vivo*

To investigate the integration of retinal input in excitatory and inhibitory neurons in the SC *in vivo*, we recorded extracellular neural activity in the visual layers of SC in VGAT-ChR2 mice using high-density Neuropixels probes (Jun et al., 2017). We employed a tangential insertion approach to maximize the extent of visually driven channels in the SC (Figure 1A) (Sibille et al., 2022a). Notably, we recently demonstrated that this approach allows us to not only measure spiking activity from SC neurons, but also to record electrical signals from retinal ganglion cell axons (RGC) that terminate in the SC (Sibille et al., 2022a). The somatic action potentials of SC neurons can be distinguished from the axonal action potentials of RGCs based on their spatiotemporal waveforms profile (Sibille et al., 2022a). RGC axonal waveforms are triphasic with a larger spatial spread (Figure 1D left) while somatic SC neurons show a characteristic biphasic waveform profile (Figure 1D, middle and right).

To study cell-type specific differences, we combined the Neuropixels recordings with an optogenetic identification strategy (optotagging) to identify GABAergic SC neurons in VGAT-ChR2-EYFP (Zhao et al., 2011) mice (Figure 1A, B; data from n = 11 experiments in n = 9 mice included in the analysis, if not stated otherwise). In these transgenic mice, GABAergic neurons specifically express Channelrhodopsin-2 and can be identified upon blue light stimulation. To photo-activate a large proportion of GABAergic SC neurons using short light pulses (100ms pulses, 2Hz, 2.7 mW) we inserted the optic fiber perpendicularly to the Neuropixels probe (Figure 1A, right, see Material and Methods). Using this recording and light stimulation configuration we could activate GABAergic SC neurons across an average of ~1.5 mm of SC tissue (light-activated range = 1.50 ± 0.41 mm, Figure 1B) which also allowed us to record SC neurons along continuous retinotopy (Figure 1C, right) in a cell-type specific manner (Figure 1G). We used the visually evoked activity and continuous retinotopy to demarcate the boundaries of the SC (Figure 1C). Moreover, for the characterization of excitatory and inhibitory classes of SC neurons, we limited our analysis to single units that were localized within the range of optogenetic stimulation (Figure 1B/C and Figure 1 – figure supplement 1A, see Material and Methods). Cell types were characterized using a custom-written graphic-user-interface (GUI, see Material and Methods) to label units that were activated by the LED pulse as inhibitory neurons (INs, Figure 1E, middle). These neurons were distinguished based on their reliable increase in firing rate in response to optogenetic stimulation during spontaneous (black screen) and visually evoked conditions (checkerboard stimulus, see Material and Methods). SC neurons that were not modulated by the LED pulses, but located within the light-activated range, were labeled as excitatory (EXNs, Figure 1E bottom). Excitatory and inhibitory SC neurons were equally distributed within the boundaries of LED stimulation for 9/11 experiments (p values = 3.07×10^{-1}, 1.15×10^{-2},

159 7.55×10^{-1}, 8.34×10^{-1}, 5.01×10^{-6}, 0.79, 0.80, 0.26, 0.33, 0.08, 0.13, Wilcoxon rank-sum test). In only
160 two experiments EXNs and INs were not equally distributed, but only 2 single units were located in
161 the region without included SC IN units, that passed the quality criteria for spike sorting (Figure 1 –
162 figure supplement 1B, see Material and Methods). As expected, retinal axons were not activated by
163 the LED pulse (Figure 1E, top), except for a few cases (4/326 RGCs) which were excluded from the
164 connectivity analysis in this study. In total, we recorded 326 RGC axons and 680 SC neurons. Among
165 the recorded SC neurons one third (31.2%) were GABAergic (Figure 1G, n = 468 EXNs, n = 212
166 INs).
167
168 Having sorted the SC neurons into the cell classes using optogenetic stimulation (EXNs and
169 optogenetically identified INs) we compared different spike waveform features to test whether SC
170 neurons show differences in their waveforms. Characterizing the spike waveforms is commonly used
171 in the cortex or hippocampus to differentiate between glutamatergic and GABAergic neurons (Lee
172 et al., 2016; Moore and Wehr, 2013; Niell and Stryker, 2008). However, the separation based on
173 differences in waveform features was not an adequate measure to separate SC EXNs from SC INs
174 (Figure 1 – figure supplement 2). This result is in line with findings by Essig et al. (2021) who did not
175 observe a cell type specific difference between waveform features in the SC (Essig et al., 2021).
176 Similar findings have been shown in the inferior colliculus (Ono et al., 2017), a neighboring midbrain
177 structure, suggesting that waveform classification analyses used in the cortex are not suitable for
178 distinguishing neurons in the midbrain.
179
180 To further characterize the response properties of the different cell classes (RGC, SC INs, SC
181 EXNs), we measured their firing rates (FR) in response to a natural movie stimulus provided in
182 Froudarakis et al. (2014) (Froudarakis et al., 2014) (see Material and Methods). We found that RGCs
183 show the highest FR (firing rate RGC: median = 7.55 spikes/s, Q1 = 2.39 spikes/s, Q3 = 17.93
184 spikes/s, n = 326 EXNs; Figure 1G, bottom). On average, the mean FR in SC INs (firing rate IN:
185 median = 3.63 spikes/s, Q1 = 1.6 spikes/s, Q3 = 8.02 spikes/s, n = 212 INs) was 1.8 times higher
186 compared to that of SC EXNs (firing rate EXN: median = 1.38 spikes/s, Q1 = 0.49 spikes/s, Q3 =
187 4.19 spikes/s, n = 468 INs; SC EXN vs SC IN $p = 3.1567\times10^{-15}$, SC EXN vs RGC $p = 4.8362\times10^{-40}$,
188 SC IN vs RGC $p = 2.738810^{-8}$, two-sided Wilcoxon rank-sum test). Our results are in line with
189 previous studies by Reid (1998, 2003) showing that RGCs show high mean firing rates (Kara and
190 Reid, 2003; Usrey et al., 1998). Moreover, from other midbrain areas it is also known that GABAergic
191 neurons show higher FRs compared to glutamatergic cells (Ono et al., 2017).
192
193 In summary, by combining Neuropixels recordings to measure the activity of RGC axons and SC
194 neurons with optogenetic identification of GABAergic SC neurons, it becomes possible to measure

monosynaptic retinocollicular connectivity *in vivo* and retinal innervation strength in a cell-type specific manner.

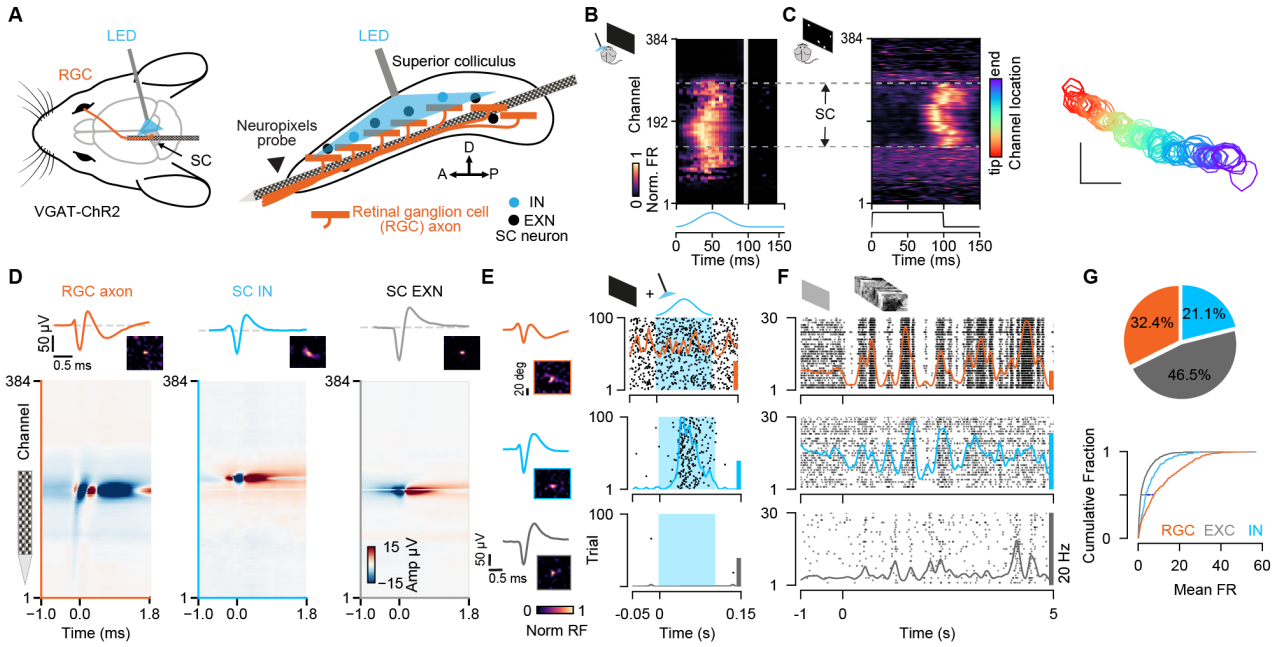

Figure 1 Simultaneous extracellular recordings of RGC axons and SC neurons combined with optotagging identifies GABAergic neurons in VGAT-ChR2 mice. A, Recording configuration for tangential electrode insertion and optotagging in the visual layers of mouse SC. The optogenetic fiber is inserted perpendicularly to the Neuropixels probe to activate GABAergic cells in VGAT-ChR2 mice. RGC afferents (orange) project onto GABAergic (blue) and non-GABAergic (black) neurons in SC. **B,** Multi-unit response (MUA) to optogenetic stimulation along the 384 recording sites during the presentation of a black screen. The large spatial extent of the optogenetic activation is evident. Gray vertical bar = light artifacts induced by the LED stimulation. **C,** Visually evoked MUA during the presentation of a sparse noise stimulus along the recording sites. Receptive field contours of recording sites with high signal-to-noise ratio. The color code reflects the location within the SC. Scale bar represents 10 degree. **D,** Spatiotemporal waveform profiles. Single channel waveforms identified at the peak channel (top) and multi-channel waveforms (bottom) for RGC axon (left, orange) and inhibitory (middle, blue) and excitatory (right, gray) SC neurons. Receptive fields (RFs) indicate visually responsive neurons. **E,** Identification of SC cell-types via optotagging. Raster plots and peri-stimulus time histograms (PSTHs) for single-neuron responses to blue light pulses (100ms) presented under baseline conditions. Excitatory SC neurons (EXNs, bottom) and RGCs (top) do not respond to the LED pulse, while GABAergic SC neurons respond to the light pulse with an increase in spiking response (middle). Optogenetic stimulation period is highlighted in blue. The colored scale bars on the right represent 20 Hz firing rate. **F,** PSTHs and raster plots for different cell types shown in E in response to a natural movie stimulus (10s, 30 trials). Note the high firing rate in RGCs. **G,** Top: Proportion of identified GABAergic (INs, blue), non-GABAergic (EXNs, gray) SC neurons and retinal axons (RGCs, orange) populations. Note that around one third of the captured SC neurons are GABAergic (n = 326 RGCs, n = 468 EXNs, n = 212 INs). Bottom: Cumulative distribution of mean firing rates in response to a natural movie stimulus presented for 10s, 30 trials. Two-sided Wilcoxon rank-sum test.

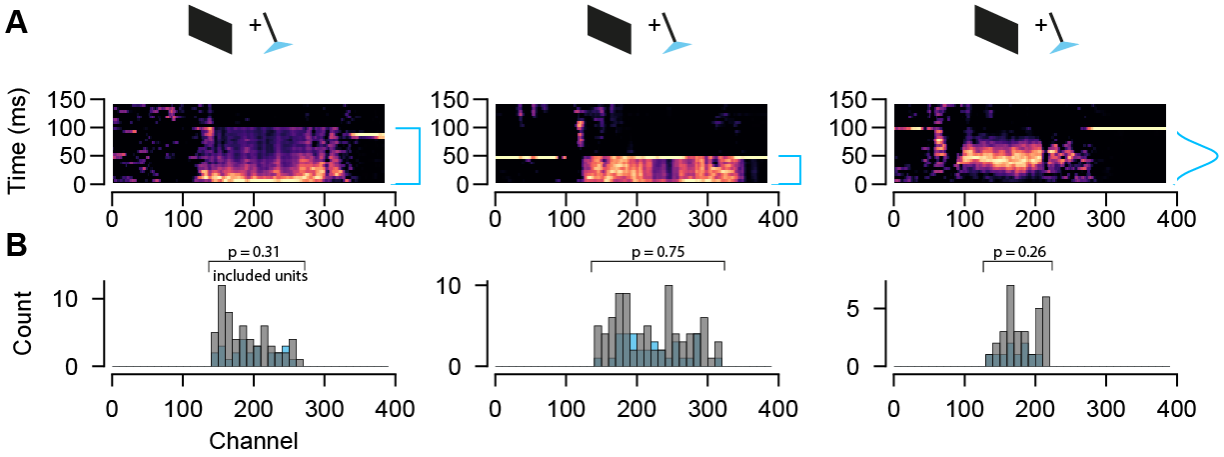

Figure 1 – figure supplement 1 Optogenetic response and spatial distribution of excitatory and inhibitory SC neurons. A, Multi-unit activity in response to optogenetic stimulation (100 or 50 ms) using a square wave pulse or a Gaussian-shaped LED pulse for three individual recordings. **B,** Spatial distribution of included excitatory and inhibitory SC single units within the range of channels that are activated via LED stimulation. Both cell types are equally distributed. Two-sided Wilcoxon rank-sum test.

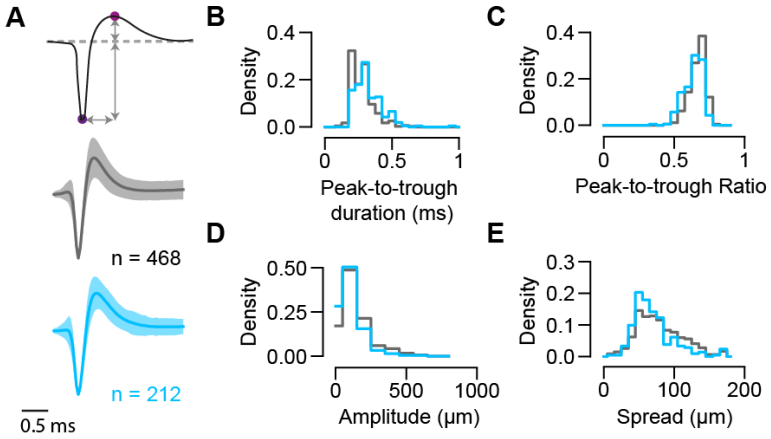

Figure 1 – figure supplement 2 Spike waveform features analysis for GABAergic and non-GABAergic neuron populations in the SC. A, Top: Illustration of features extracted from single-channel waveforms (magenta circles indicate the trough and peak). Middle and bottom: Single-channel mean waveforms for non-GABAergic (gray; n = 468) and GABAergic (blue, n = 212, n = 9 mice) SC populations (mean±SEM). **B-D,** Distribution of waveform features extracted from single-channel waveforms for inhibitory and excitatory SC populations. Peak-to-trough duration represents the time between trough and peak ($p = 4.05\times10^{-10}$). Peak-to-trough ratio represents the ratio between amplitudes of peak and trough ($p = 4.45\times10^{-9}$). Amplitude is the absolute difference between trough and peak ($p = 1.38\times10^{-9}$). **E,** Distribution of waveform spread along the probe extracted from multichannel waveforms for GABAergic and non-GABAergic SC populations ($p = 1.58\times10^{-4}$, n = 468 EXNs, n= 212 INs, Two-sided Wilcoxon rank-sum test).

Retinal input integration in excitatory and inhibitory SC neurons

To study the monosynaptic retinocollicular connectivity *in vivo* and retinal innervation strength, we identified putative monosynaptically connected RGC-SC pairs employing established cross-correlation analysis (CCG) methods (Alonso et al., 2001; Bereshpolova et al., 2020; Sibille et al., 2022a). A significant transient and a short-latency peak in the spike train CCG is a hallmark of monosynaptic connectivity (Figure 2A) and identifies connected RGC-SC pairs. We measured up to 98 monosynaptic connections in individual recordings, depending on the number of measured RGC axons (Figure 2C). In total, we identified 305 connected RGC-SC pairs, of which 29.8% were retinal axons that connected onto GABAergic SC neurons (n = 214 connected RGC-SC EXN pairs, n = 91 connected RGC-SC IN pairs, Figure 2B/D). This high yield in monosynaptically connected pairs was due to the close proximity of the simultaneously recorded RGC axons and SC neurons on the high-density electrode (Figure 2D, bottom) (Sibille et al., 2022a). For most of the connected RGC-SC pairs the peak channels on the electrode were on average 50-60 µm apart on the probe and hence within SC (distance RGC-EXN: median = 40.0 µm, first quartile = 25.61 µm, third quartile = 62.1 µm; distance RGC-IN: median = 51.22 µm, first quartile = 32.0 µm, third quartile = 83.08 µm). We found a significant difference in peak channel distance between RGC-SC EXN and RGC- SC IN pairs with longer distances between RGC axons and inhibitory SC neurons ($p = 0.03287$, two-sided Wilcoxon rank-sum test), however, the effect size was small (Cohen's $d = 0.0915$). The maximum distance for retinal axons and inhibitory SC neurons was 240 µm, while the peak channels of one RGC-SC EXN pair were 960 µm apart. The latter pair might include a SC wide field neuron as these cells are excitatory and their dendritic arbor widths have been reported to spread up to 900 µm (Gale and Murphy, 2014).

To assess the connection strength between RGCs and excitatory and inhibitory SC neurons, we calculated the connection efficacy (Usrey et al., 1999). The efficacy measures the connection strength as the probability of an RGC spike triggering an action potential in the postsynaptic SC neuron (see Material and Methods). We found highly diverse connectivity patterns for RGC-SC EXC and RGC-SC IN pairs. RGC activity evoked robust firing in both SC cell types (Figure 2E, top), however, pairs with weak connection strength were also observed as recently described in Sibille et al. (2022a) (Figure 2E, bottom). Across the population, both SC cell types received similarly strong input from the retina (efficacy RGC-SC IN: median = 4.54 %, Q1 = 2.2 %, Q3 = 7.96 %, maximum = 62.05 %, n = 91 connected pairs; efficacy RGC-SC EXN: median = 3.5 %, Q1= 1.96 %, Q3 = 5.89 %, maximum = 41.12 %, n = 214 connected pairs; Figure 2F). While we observed a tendency for slightly stronger RGC-SC IN connections, this difference was not statistically significant ($p = 0.053$, two-sided Wilcoxon rank-sum test). To assess whether the connectivity strength is related to the firing of the postsynaptic cell, we examined the relationship between the efficacy and the overall firing rate throughout the entire recording session. Surprisingly, our results demonstrate a positive

correlation between the efficacy and the mean firing rate on the population level (Figure 2G, RGC-SC EXN r = 0.42685; p < 0.0005; RGC-SC IN: r = 0.43543, p = 0.00002, two-sided Wilcoxon rank-sum test).

Here, we set out to explore how RGC spikes drive the activity in postsynaptic excitatory and inhibitory SC neurons. We did not find a cell-type specific difference in connection strength and therefore conclude that inhibitory and excitatory SC neurons are innervated comparably strong and are both reliably driven by their retinal inputs.

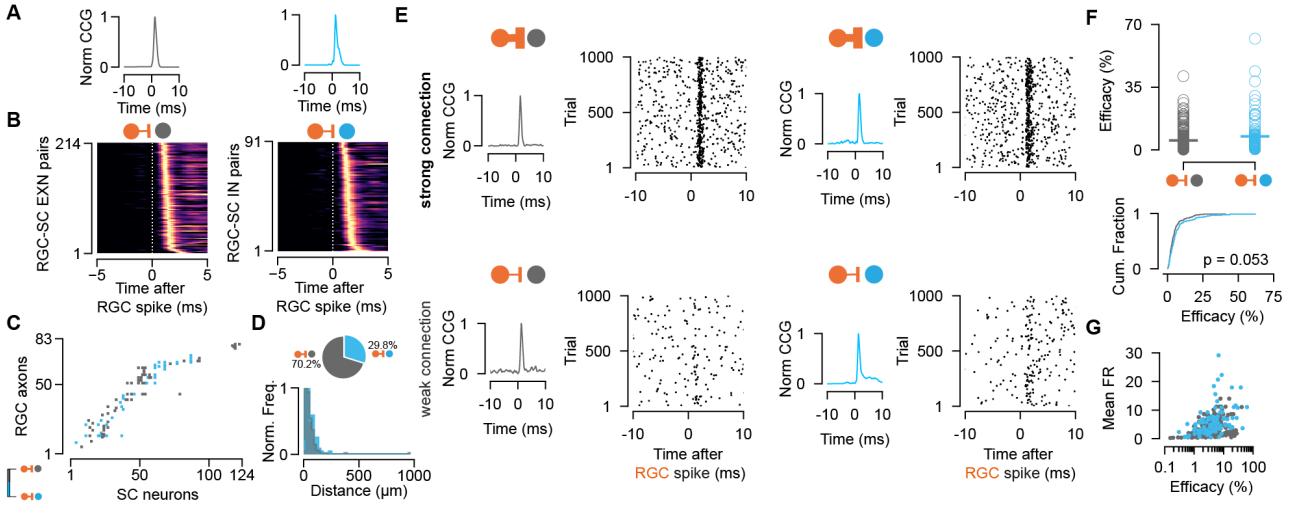

Figure 2 Retinal innervation is similarly strong to excitatory and inhibitory SC neurons. A, Monosynaptically connected RGC-SC EXN (gray) and RGC-SC IN (blue) pairs are identified via cross-correlation analysis (CCG). **B,** CCGs of connected RGC-SC EXN and RGC-SC IN pairs sorted by their peak latency (n = 214 RGC-SC EXN, n = 91 RGC-SC IN, n= 11 recordings). **C,** Connectivity matrix from a single recording. Gray marks indicate connections onto excitatory SC neurons, blue marks indication connections onto inhibitory SC neurons. RGC axons and SC neurons are sorted by their peak channel along the electrode. **D,** Distribution of peak channel distances between RGC axons and connected SC neurons (p = 0.0328, two-sided Wilcoxon rank-sum test). Inset shows pie chart of identified RGC-SC IN and RGC-SC EXN pairs. **E,** Elicited SC spiking in response to firing of a presynaptically connected retinal ganglion cell (RGC). Raster plot shows SC firing to 1000 randomly selected RGC spikes. Both SC cell types show robust activation upon RGC spiking (top) but also weaker connections can be found (bottom). **F,** Scatter plot and cumulative distribution of synaptic efficacy as a measure for connection strength for RGC-SC EXN and RGC-SC IN connected pairs (p = 0.053, n = 214 RGC-SC EXN, n = 91 RGC-SC IN). **G,** Efficacy as a function of mean FR during the entire recording session (RGC-SC EXN r = 0.42685; p < 0.0005; RGC-SC IN: r = 0.43543, p = 0.00002). Two-sided Wilcoxon rank-sum test.

Functional similarity of retinocollicular connections

In sensory cortices, inhibitory neurons are less selective and receive a diverse and nonspecific set of thalamic inputs compared to excitatory neurons which receive more specific thalamic inputs (Alonso and Swadlow, 2005; Bruno and Simons, 2002). However, the selectivity and functional similarity between RGCs and their excitatory and inhibitory target populations in SC remains largely unknown (Shi et al., 2017). Despite both SC populations showing a similar innervation strength from retinal axons, inhibitory neurons could sample from a more functionally diverse population of RGCs. To test this, we characterized the functional similarity between the RGCs and their connected postsynaptic SC neurons. To this end, we calculated the correlation coefficients between the trial-averaged visually evoked activity of connected RGC-SC pairs in response to light and dark sparse noise stimuli (r_{SL} & r_{SD}) as well as the natural movie stimulus (r_{NM}), a phase scrambled version (r_{PSM}) and a checkerboard stimulus (r_{Chk}) (Figure 3A/B, RGC-SC with high signal-to-noise in their receptive field, see Material and Methods). To quantify the overall functional similarity by a single similarity value, we averaged the five correlation measurements (similarity = (r_{SL}+ r_{SD} + r_{NM}+ r_{PSM} + r_{Chk})/5). A similarity value of 1 corresponds to perfectly correlated visually driven responses between the RGC and the postsynaptic SC neuron, while a value of 0 signifies uncorrelated responses. In our data, the RGC-SC pairs span a wide range of functional similarity, however, we found no significant difference between RGC-SC EXN and RGC-SC IN pairs (similarity for RGC-SC EXN = 0.44 ± 0.15 and RGC-SC IN = 0.37 ± 0.19, n = 85 RGC-SC EXN pairs, n = 29 RGC-SC IN pairs, p = 0.245, two-sided Wilcoxon rank-sum test, Figure 3B). In a next step, we correlated the connection efficacy measure to the similarity index. The synaptic efficacy was positively correlated with the functional similarity of the connected pairs, with a stronger correlation for RGC-SC IN pairs (RGC-SC EXN r = 0.37, p = 0.0005; RGC-SC IN r = 0.44, p = 0.02, Figure 3C). Overall, we observed that functionally similar pairs are more strongly connected. However, we also observed cases of relatively strong connected RGC-SC pairs (~10%) with low similarity (Figure 3C), suggesting that some SC neurons receive convergent input from a functionally more diverse pool of RGC afferents (Sibille et al., 2022a). Our findings delineate that both RGC-SC EXN and RGC-SC IN connected pairs are organized, while functionally similar properties between the pre- and postsynaptic neuron are reflected in a stronger connection.

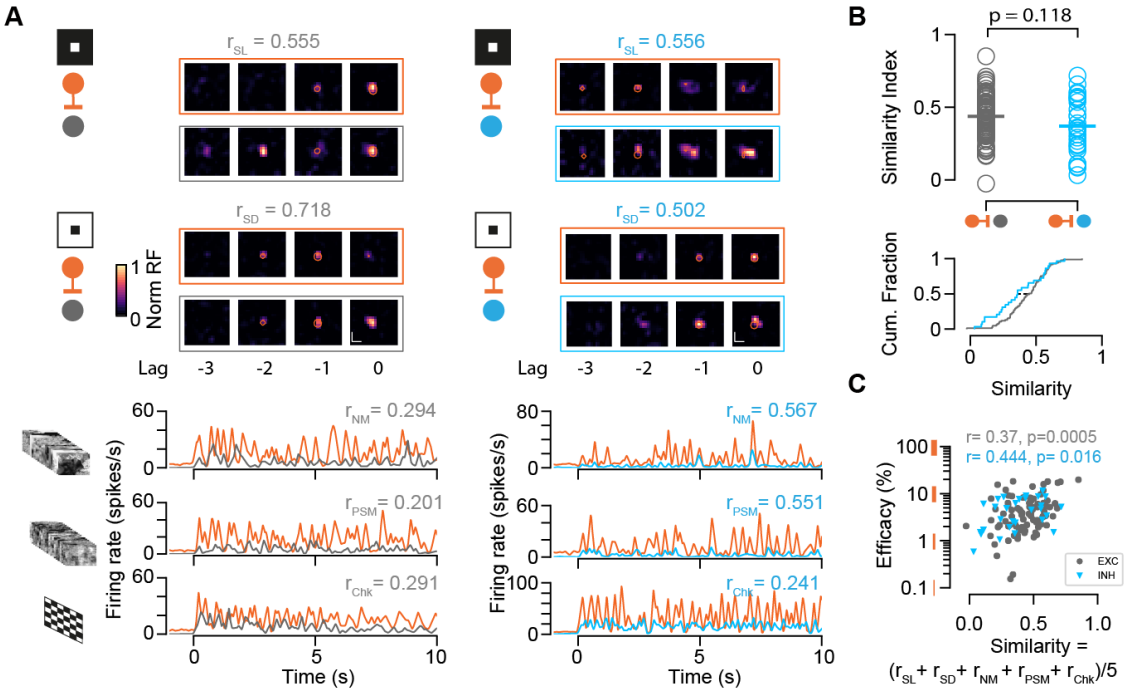

Figure 3 Characterization of functional similarity between retinocollicular connected pairs. A, Top: Spatiotemporal receptive fields (STRF) evoked by dark (SD) and light (SL) sparse noise stimuli for RGC-SC EXN and RGC-SC IN connected pairs. Bottom: Visually evoked activity in response to a natural movie (NM), phase scrambled movie (PSM) and dense noise (Chk) stimulus. The functional similarity of the RGC axon and the postsynaptic SC neuron is characterized by the correlation coefficient during the different stimuli conditions (r_{SD}, r_{SL}, r_{NM}, $r_{PSM,}$ r_{Chk}). **B,** The overall functional similarity between the presynaptic RGC and the postsynaptic SC neurons is reflected in the similarity index calculated from the averaged correlation coefficients ($r_{SL} + r_{SD} + r_{NM} + r_{PSM} + r_{Chk}$)/5 (p = 0.118, two-sided Wilcoxon rank-sum test, n = 85 RGC-SC EXN pairs, n = 29 RGC-SC IN pairs). Scatter plot (top) and cumulative distribution (bottom) of similarity index. **C,** Relationship between similarity index and connection efficacy (Pearson correlation coefficient; n = 85 RGC-SC EXN pairs, n = 29 RGC-SC IN pairs).

Paired-spike interactions of the retinocollicular connections

We showed that retinal spikes are efficient in driving SC activity for both excitatory and inhibitory neurons. As the timing of presynaptic activity has been assessed as a parameter that modulates postsynaptic firing (Zucker, 1989) and connection strength (Kara and Reid, 2003; Usrey et al., 1998), we wanted to know whether the temporal pattern of retinal activity has different effects on the synaptic efficacy of excitatory and inhibitory SC neurons. To that end, we studied the short-term dynamics (facilitation or depression) of the measured connections and performed a paired-spike analysis approach as described by Usrey and colleagues in 1998 (Usrey et al., 1998). A pair of retinal spikes (1^{st}, 2^{nd} RGC) was defined by its temporal firing patterns: inter-spike interval (ISI) and dead time. We selected RGC spikes for which a 1^{st} RGC followed the 2^{nd} RGC by a specific ISI (minimum ISI = 5ms, maximum ISI = 30ms). The dead time ensures that the 1^{st} RGC was preceded by a minimum period without activity (30ms) (Figure 4A).

We found that overall 2^{nd} retinal spikes were more efficient in driving SC activity, and thus facilitating. This was true for both RGC-SC EXN (efficacy 1^{st} RGC: median = 1.8 %, Q1 = 0.77 %, Q3 = 4.47 %; efficacy 2^{nd} RGC: median = 2.66 %, Q1 = 1.16 %, Q3 = 6.07 %, p 1^{st} vs 2^{nd} = 3.13×10^{-25}, n = 214 pairs) and RGC-SC IN connected pairs (efficacy 1^{st} RGC: median = 3.66 %, Q1 = 1.6, Q3 = 8.61; efficacy 2^{nd} RGC: median = 4.33, Q1 = 2.03, Q3 = 8.25, p 1^{st} vs 2^{nd} = 1.68×10^{-6}, n = 91 pairs, Wilcoxon signed-rank test) (Figure 4B, C). This effect is known as paired-spike enhancement and has been reported earlier in retinogeniculate (Mastronarde, 1987; Usrey et al., 1998) and geniculocortical (Usrey et al., 2000) connections. The majority of retinocollicular connected pairs showed paired-spike enhancement where 2^{nd} retinal spikes were more effective in driving SC response (86.45% (185/214) RGC-SC EXN pairs, 80.22 % (73/91) RGC-SC IN pairs). The effect was more pronounced in RGC-SC EXN pairs where the 2^{nd} retinal spike was 1.7 times as effective in driving responses in the postsynaptic SC neuron, while for RGC-SC IN pairs, the 2^{nd} retinal spike was only 1.3 times more efficacious in driving SC spiking. To quantify this observation, we calculated the paired-spike ratio (PSR = efficacy 2^{nd}/efficacy 1^{st}) which confirmed a higher facilitation effect for RGCs connecting into excitatory neurons (PSR RGC-SC EXN = 1.711 ± 1.14; RGC-SC IN: 1.281 ± 0.414, p = $2{,}58 \times 10^{-7}$, Wilcoxon rank-sum, n = 305 pairs, Figure 4D).

Previous work in the thalamocortical system has shown that weaker synaptic connections can be more strongly modulated compared to stronger synaptic connections (Ferrarese et al., 2018). To test the notion that also in the retinocollicular system, connected pairs with lower efficacy in response to 1^{st} RGCs show greater enhancement in response to the 2^{nd} RGCs, we correlated the efficacy of the 1^{st} RGC to the PSR (Figure 4E). We observed a negative correlation between the logarithm of the 1^{st} RGC efficacy and the logarithm of PSR for both RGC-SC EXN (r = 0.3314, p = 7.0148×10^{-7}, n = 214 pairs) and RGC-SC IN pairs (r = 0.4767, p = 1.7714×10^{-6}, n = 91 pairs). However, we found pairs that show low efficacy in response to the 1^{st} RGC and low PSR. Taken together, we observed paired-spike enhancement in RGCs connecting onto both inhibitory and

excitatory SC neurons, with a stronger facilitation effect for retinal afferents connecting onto excitatory, in comparison to inhibitory, SC target neurons. To estimate whether the ISI interval has an effect on the PSR, we added another group of 2-30 ms ISI interval to include RGCs that fire at high frequencies (PSR RGC-SC EXN = 1.783 ± 1.23; RGC-SC IN: 1.295 ± 0.528, $p = 7.03 \times 10^{-6}$, Wilcoxon rank-sum, n = 305 pairs, Figure 4F). However, we did not observe a clear difference between the 2-30 and 5-30 ms groups for inhibitory connections (SC IN: p = 0.604, Wilcoxon signed-rank test). In contrast, the two different ISI groups of excitatory neurons show a statistically significant difference (p = 0.011, Wilcoxon signed-rank test), however, the effect size is small (Cohen's d RGC-SC EXN = 0.063, RGC-SC IN = 0.030).

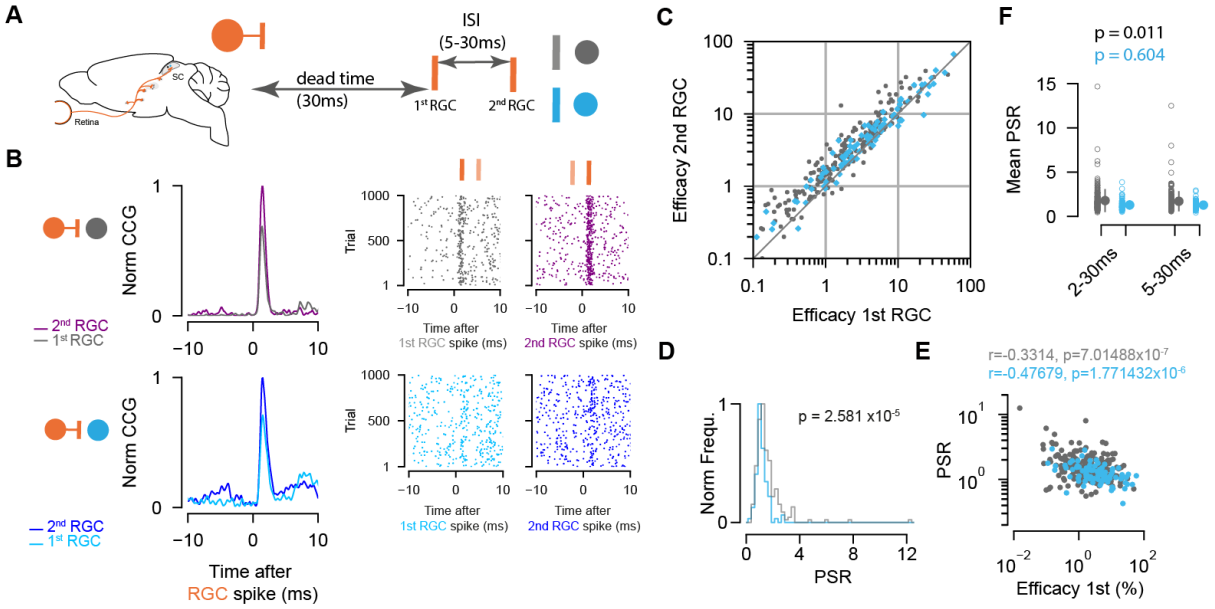

Figure 4 Paired-spike dynamics: Second retinal spikes are more efficient in driving SC response.

A, Schematic illustrating the temporal dynamics between two successive RGC spikes. Pairs of RGC spikes with a minimum inter-spike interval (ISI) of 5 ms and maximum ISI of 30 ms were included if there were no preceding spikes before the 1st RGC for a dead time of at least 30ms. **B,** Cross-correlograms (CCG) of example RGC-SC EXN and RGC-SC IN pairs calculated from spike trains selected for 1st and 2nd RGCs and the corresponding raster plots to 1000 trials triggered on RGC spikes. **C,** Scatter plot of efficacies for 1st versus 2nd retinal spikes. The majority of connected pairs (185/214 RGC-SC EXN pairs; 73/91 RGC-SC IN pairs) showed paired-spike enhancement in response to 2nd RGC spikes. **D,** Distribution of paired-spike ratio (PSR) for RGC-SC EXN and RGC-SC IN connected pairs. The paired pulse enhancement is stronger in SC-EXNs (n = 214 RGC-SC EXN; n = 91 RGC-SC IN, $p = 2.581 \times 10^{-5}$, two-sided Wilcoxon rank-sum test). **E,** Correlation of 1st RGC efficacy with the PSR for connected pairs (r = 0.3314 for n = 214 RGC-SC EXN pairs and r = 0.4767 for n = 91 RGC-SC IN pairs; logarithmic values; Pearson correlation coefficient test). **F,** Change in mean PSR depending on ISI for different groups of ISI intervals (2-3 ms and 5-30ms). The 2-30 ms group ensures to include high-firing RGCs (RGC-SC EXN pairs 2-30 vs. 5-30 ms p = 0.011; RGC-SC IN pairs 2-30 vs. 5-30 ms p = 0.604; Wilcoxon signed-rank test).

Inhibitory SC neurons are less coupled to the retina compared to excitatory SC neurons

Our data so far reveals that excitatory and inhibitory SC neurons receive similarly strong drive from their retinal afferents. However, we observed a higher mean firing rate in SC INs compared to SC EXNs, on average (Figure 1G), which is intriguing given the similarity in the RGC drive on both cell types. A possible explanation could be that the activity of SC INs is less coupled to the RGC inputs as compared to that of SC EXNs, i.e. SC INs spikes are less often driven by their RGC inputs. To examine how strongly the activity of the two populations of SC neurons is coupled to the activity of individual RGC inputs, we estimated the synaptic coupling strength from the connection contribution (Levick et al., 1972; Sibille et al., 2022a; Usrey et al., 1999) of the measured retinocollicular pairs. The connection contribution reflects the fraction of postsynaptic SC spikes that are preceded by a presynaptic retinal spike within a short time window (Figure 5A). High contribution values indicate that SC neurons are primarily driven by individual RGC afferent inputs, while low contribution values point towards an integration of multiple inputs.

Interestingly, we found that the contribution of individual retinal spikes on SC activity was higher for excitatory compared to inhibitory SC neurons (Figure 5B) (contribution RGC-SC EXN: median = 18.27% Q1 = 10.79%, Q3 = 29.69%, n = 214; contribution RGC-SC IN: median = 12.2%, Q1 = 6.61%, Q3 = 23.02%, n = 91 connected pairs, p = 0.0003, two-sided Wilcoxon rank-sum test). This opens up the possibility that SC EXNs might be more specifically linked to the retinal input compared to SC INs. To assess the relationship between the coupling strength and the functional similarity, we correlated both measures and found a positive correlation, suggesting that stronger coupled pairs show higher similarity (RGC-SC EXN r = 0.541, p = 8.9×10^{-8}, n = 85 pairs; RGC-SC IN (r = 0.461, p = 0.012, n = 29 pairs, Pearson correlation coefficient test, Figure 5C). Moreover, we observed a diversity of firing rates in both SC EXNs and SC INs (Figure 1G) which suggests that low contribution values are related to the mean firing rates of the SC neurons. And indeed, when we correlated the contribution to the mean firing rate, we found a negative correlation for both RGC-SC EXN and RGC-SC IN pairs (RGC-SC EXN r = -0.15079, p = 0.02742; RGC-SC IN r = -0.48386, p < 0.00000, Pearson correlation coefficient test n = 214 RGC-EXN; n = 91 RGC-IN connected pairs) (Figure 5D and Figure 5– figure supplement 1).

Taken together, the cell-type specific difference in retinal coupling strength suggests that retinal input contributes a substantial part to the spiking activity of excitatory SC neurons, while inhibitory SC neurons seem to also integrate inputs from other sources. This finding denotes that excitatory SC neurons are more tightly linked to the retinal input compared to inhibitory SC neurons.

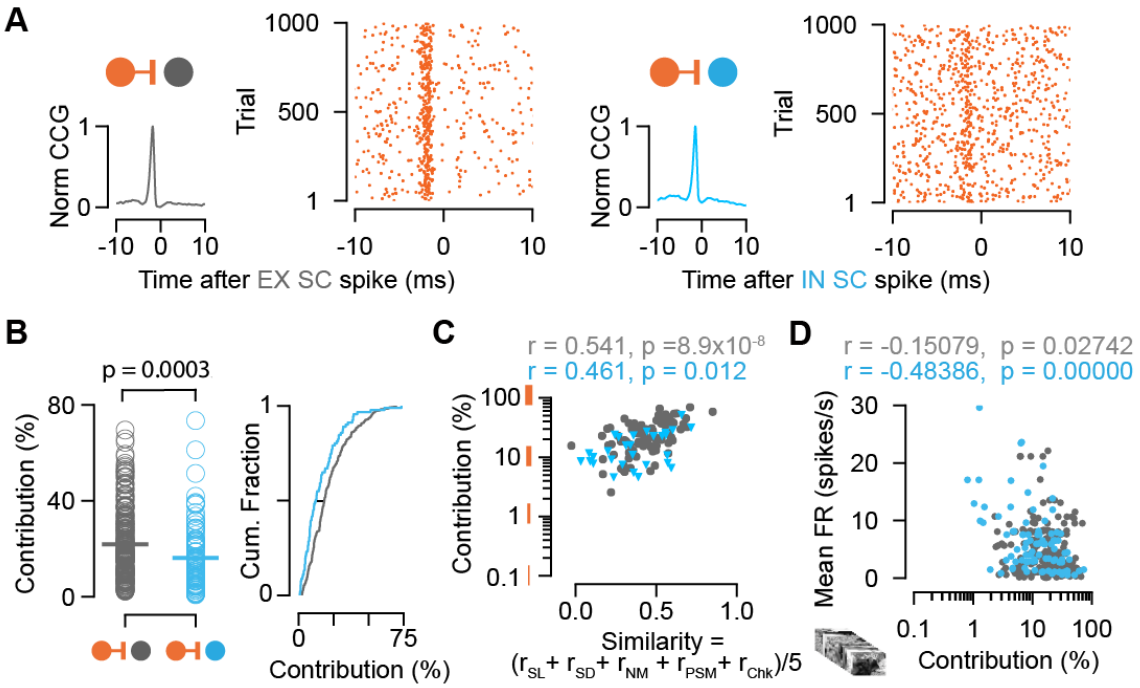

Figure 5 Connection contribution is higher in connected RGC-SC EXN pairs. A, Example CCGs of monosynaptically connected RGC-SC EXN (top) and RGC-SC IN (bottom) pairs. Connected pairs were identified by their peaks in the CCGs (left). Raster plots of RGC spiking activity triggered on 1000 SC spikes (right). **B,** Scatter plot and cumulative distribution of contribution values for RGC-SC EXN and RGC-SC IN pairs (n = 114 RGC-SC EXN pairs, n=91 RGC-SC IN pairs, p = 0.0003, two-sided Wilcoxon rank-sum test). **C,** Relationship between functional similarity index and connection contribution (Pearson correlation coefficient test; n = 85 RGC-SC EXN pairs, n = 29 RGC-SC IN pairs). **D,** Correlation of mean firing rate (to natural movie stimulus) and contribution for RGC-SC EXN and RGC-SC IN pairs (Pearson correlation coefficient, two-sided Wilcoxon rank-sum test, n = 214 RGC-EXN and n = 91 RGC-IN connected pairs; n = 11 penetrations from 9 mice).

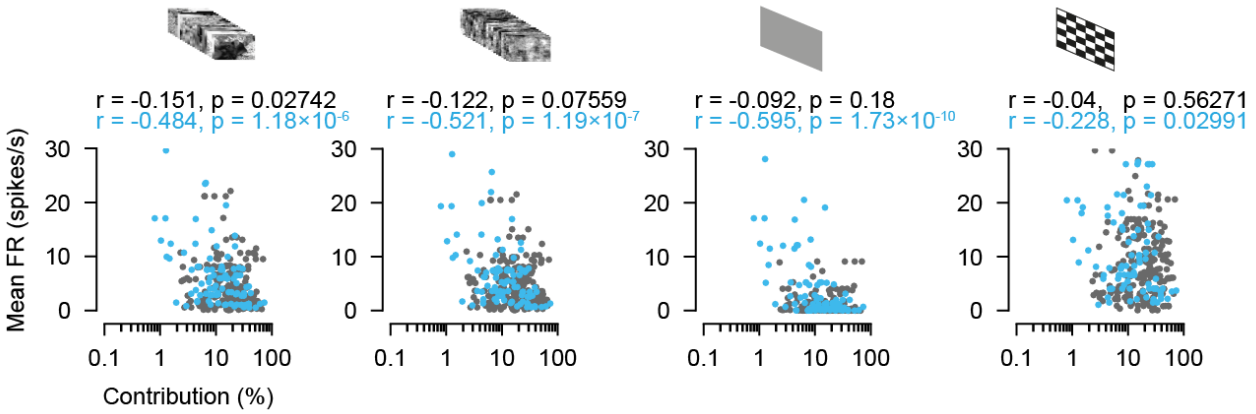

Figure 5 – figure supplement 1 Contribution as a function of firing rate during different stimulus conditions. Relationships between contribution and the conditions during natural movie (NM), phase scrambled movie (PSM), gray background (Bkg) and checkerboard (Chk) for RGC SC EXN and RGC-SC IN pairs RGC-SC EXN n = 214 pairs, RGC-SC INH n = 91 pairs, two-sided Wilcoxon rank-sum test).

DISCUSSION

In this study, we elucidate how inhibitory and excitatory SC neurons integrate visual information from the retina *in vivo*. By combining the tangential Neuropixels recording approach with optotagging techniques, we were able to measure RGC-SC connected pairs in a cell-type specific manner and study their functional organization. Our findings allow the following conclusions: (1) The retinal drive is similarly strong for RGCs connecting onto GABAergic and non-GABAergic SC neurons. (2) The connection strength between the RGCs and both SC cell classes is positively correlated with their functional similarity, while still allowing for the presence of strong connections with low functional similarity. (3) Paired-spike enhancement in RGC-SC connections was a signature for both excitatory and inhibitory SC neurons. Finally, (4) the contribution of a retinal spike to overall SC firing is higher in excitatory SC neurons compared to inhibitory SC neurons.

We studied retinocollicular connectivity strength and aimed to answer the question whether excitatory and inhibitory SC populations use similar or different coding schemes to integrate visual information compared to the thalamocortical visual system. Connectivity patterns and circuit motifs have been extensively studied in the thalamocortical system, yet our understanding of the encoding mechanisms that govern retinocollicular signaling remains rudimentary albeit recent studies suggest that feedforward inhibition might be at play (Villalobos et al., 2018; Whyland et al., 2020). While cortical inhibitory neurons are more strongly activated by thalamic axons compared to excitatory neurons (Bruno and Simons, 2002; Cruikshank et al., 2007; Ji et al., 2016), our results now show that in the SC, the afferent retinal drive is comparably strong on excitatory and inhibitory neurons. This finding is intriguing and suggests that the two major visual brain structures in the vertebrate brain, the visual cortex and the SC, integrate afferent sensory information differentially.

Several parameters for example the degree of convergence (Kara and Reid, 2003), response properties (Alonso et al., 2001), synaptic mechanisms (Cruikshank et al., 2007) or spiking patterns (Usrey et al., 1998) can have meaningful effects on modulating the input strength on the target cell. SC neurons receive input from a small number (4-6) of RGCs (Chandrasekaran et al., 2007; Furman et al., 2013). In contrast, cortical neurons receive numerous (approximately one order of magnitude more) thalamic inputs that are usually weak (Bruno and Sakmann, 2006; Jin et al., 2011; Lien and Scanziani, 2018). Overall, we observed strong retinal drive onto both SC populations indicated by high efficacy values (Figure 2), and thus individual inputs may be sufficiently strong to drive the SC neuron. This is in contrast to thalamocortical inputs, where individually efficacy values are low, but the thalamic drive is boosted by synchronously active thalamic inputs (Alonso et al., 1996; Bruno and Sakmann, 2006). Our recording method allows for the simultaneous recording of multiple RGC afferents from SC neurons making it possible to evaluate how the synchrony among RGC afferents modulates the firing of postsynaptic SC neurons in future studies.

The difference in connection strength between cortical excitatory and inhibitory neurons could be partly attributed to their differences in response properties. Cortical inhibitory neurons display higher sensitivity, receive more convergent thalamic input, have higher firing rates and sample more randomly while excitatory neurons receive highly functional specific thalamic input (Kyriazi et al., 1994; Reid and Alonso, 1995; Simons and Carvell, 1989). While we observed higher firing rates in inhibitory SC neurons (Figure 1G), the efficacy of the RGC-SC connections was comparable between both types of neurons (Figure 2F), suggesting that the sensitivity of both neuron types is not markedly disparate. In general, visual response properties between excitatory and inhibitory neurons in the SC may not differ to such a great extent (Inayat et al., 2015; Kasai and Isa, 2016; Shi et al., 2017), (but see (Barchini et al., 2018; Li and Meister, 2022)), and experiments in the inferior colliculus show that GABAergic and glutamatergic cells share similar response properties (Ono et al., 2017). These observations imply that in the SC and other parts of the midbrain, the cell-type specific difference in terms of selectivity might not be as strongly separated as in the cortex. Future studies are required to deeper investigate the differences in response properties of the subclasses of SC neurons and whether these properties are correlated to the RGC-SC connection strength. The positive correlation between efficacy and overall mean firing rate (Figure 2G), is intriguing. It suggests that highly excited SC neurons may transmit RGC inputs more efficaciously. Interestingly, Jouhanneau et al. (2018) reported a negative correlation between the distance of the excitatory postsynaptic potential peak to the action potential threshold and the efficacy (synaptic gain) in cortical PV neurons (Jouhanneau et al., 2018). Unfortunately, due to the inherent limitations of our extracellular recording approach, we are unable to investigate this aspect in our dataset. These findings underscore the complexity of synaptic transmission and wiring specificity and the multiple factors by which it can be influenced.

In our results, we observed an overall trend that functionally similar RGC-SC pairs show stronger connections which was true for both excitatory and inhibitory pairs (Figure 3). However, we also found pairs with considerably strong retinocollicular connectivity (efficacy values >10%) albeit the functional similarity between these connected cells was low (Figure 3C). This observation suggests that SC neurons may either show high projection-specificity by integrating inputs from a functional homogeneous population of RGCs (Li and Meister, 2022; Shi et al., 2017; Sibille et al., 2022a) or receive diverse inputs from multiple functional RGC types (Li and Meister, 2022; Sibille et al., 2022a). Moreover, a high degree of projection-specificity was recently shown to be maintained even disynaptically towards brain regions downstream of the SC (Reinhard et al., 2019), suggesting that at least one important role of the RGC-SC projection is to preserve the representation of the functionally diverse retinal channels (Baden et al., 2016). In our study, we investigated the functional similarity between connected RGC-SC pairs in response to sparse and dense noise stimuli as well as natural movie stimuli. And while we observed a diversity among the similarities between RGCs

548 and connected targets in SC, supporting the idea that SC neurons may follow diverse wiring motifs
549 (Sibille et al., 2022a), we observed no clear difference between inhibitory and excitatory SC neurons
550 (Figure 3B). To further address the influence of functional properties on wiring mechanisms, it would
551 be interesting to target the pool of distinct RGC types and to study how strongly they recruit SC
552 subpopulations and modulate postsynaptic responses of their targets.
553
554 Temporal dynamics of presynaptic activity patterns are known to play a role in modulating synaptic
555 strength (Usrey et al., 1998; Zucker, 1989). To study how the temporal spiking pattern of the RGC
556 activity shapes RGC-SC connectivity, we analyzed the paired-spike dynamics. Across the
557 population, we found a facilitating effect where responses to 2nd retinal spikes were more efficient in
558 driving SC activity for both SC neuron populations. However, the paired-spike enhancement was
559 more pronounced for excitatory than inhibitory neurons (Figure 4). Moreover, our observation
560 highlights differences in the encoding strategies used by different regions of visual processing. While
561 retinogeniculate connections show paired-spike enhancement (Usrey et al., 1998), thalamocortical
562 and corticotectal synapses express mostly depressing dynamics (Bereshpolova et al., 2006;
563 Swadlow et al., 2002; Swadlow and Gusev, 2001), but see (Usrey et al., 2000). Our data now reveals
564 that retinocollicular connections facilitate, suggesting that the temporal integration of RGC inputs by
565 SC neurons may be similar to the visual thalamus (dorsal lateral geniculate nucleus “dLGN”). The
566 dLGN serves as another main target of RGC axons, however, in the mouse, the dLGN mainly
567 consists of relay neurons, and only approximately 6% of inhibitory neurons (Butler, 2008; Evangelio
568 et al., 2018). This disparity in interneuron density makes it challenging to directly compare the SC
569 and dLGN circuits. Despite this difference, there exists a common synaptic motif between the dLGN
570 and the SC. RGC axons innervating the dLGN form triadic arrangements with excitatory and
571 inhibitory neurons (Sherman, 2004; Wilson et al., 1984) and this arrangement can also be found in
572 the SC (Whyland et al., 2020). It has been shown that GAD67 is a suitable marker to target the
573 inhibitory neurons involved in the triadic motif in the SC (Whyland et al., 2020) and therefore, it would
574 be interesting to study retinal connectivity in the context of these triads in the SC using GAD67 mice.
575
576 In our study, we used cross-correlograms that were calculated from spike trains throughout the full
577 recording period, to be applied on different connectivity strength measures. However, paired-spike
578 dynamics are known to be modulated by the local temporal structure of inputs, for example the visual
579 stimulus presented (Usrey et al., 1998). In addition, facilitating and depressing effects can change
580 with the target population (Bereshpolova et al., 2006). Further studies are required to investigate
581 whether the facilitating effect observed in our study changes upon targeting defined collicular
582 subpopulations that may have differences in firing rates or during different stimulus conditions (e.g.
583 spontaneous and stimulus evoked). In this study, retinocollicular connectivity was measured in
584 anesthetized conditions. For future studies it would be interesting to examine connectivity dynamics

and innervation strength in awake conditions as it has been shown that retinocollicular synapses are modulated by the animals' level of arousal (Schröder et al., 2020). Likewise, more than 30 different types of RGCs have been characterized (Baden et al., 2016; Sanes and Masland, 2015) and understanding how specific RGC types relay information onto the different SC neuron types would be important to address in more detail in future studies. Moreover, previous studies have shown a relationship between the response properties of SC neurons and their location along the dorsal/ ventral axis (Liu et al., 2023) and differences in the density and size of retinocollicular terminals along this axis (Carter et al., 1991). Exploring this aspect further utilizing a vertical recording approach could provide valuable insights in the context of functional organization.

Despite our observation that retinal drive is similarly strong onto both SC cell types, the contribution of retinal activity to individual SC neurons firing was higher in excitatory SC neurons. This opens up the possibility that excitatory SC neurons may be more specifically linked to retinal inputs, while inhibitory SC cells might receive excitation from other sources aside from the retina. This finding raises the question on what other sources could drive spiking in inhibitory SC neurons?

1) RGCs provide the main input to the superficial SC (Ellis et al., 2016) with limited convergence (Sibille et al., 2022a). Nonetheless, the convergence may be higher for RGCs connecting onto inhibitory SC neurons which could explain the lower contribution and higher mean firing rates we found in inhibitory neurons. However, it has to be considered that our *in vivo* recording technique is limited in capturing the total pool of converging RGC inputs onto a neuron (Sibille et al., 2022a). Moreover, it has been shown that different types of RGCs exhibit variations in their axonal diameter, and this diameter is associated with how these cells relay information (Perge et al., 2009). As a result, our recording approach may have a tendency to capture signals from RGCs with high firing rates that are located in close proximity to the Neuropixels probe. Viral retrograde transsynaptic tracing methods (Muellner and Roska, 2023; Rompani et al., 2017), could be employed to study the full presynaptic RGC pool of single SC neurons.

2) In addition to retinal inputs, the SC receives extensive projections from the visual cortex (V1) that could act as a potential candidate to excite inhibitory neurons. And while indeed GABAergic horizontal cells have been shown to receive V1 input (Zingg et al., 2017), the majority (93%) of corticotectal terminals target the dendrites of non-GABAergic neurons in the SC (Masterson et al., 2019). Therefore, more work is needed and studying V1 excitation to defined inhibitory SC subpopulations will be an important topic to be investigated by the use of tracing studies and will shed light into this complexity.

3) Intracollicular connections can provide a source of recurrent excitation on SC neurons, amplifying the retinal drive (Shi et al., 2017). However, the cell-type specificity of the intracollicular amplification is still debated. For example, while GAD2-positive horizontal cells receive excitatory inputs from stellate cells (Gale and Murphy, 2018), intracollicular connectivity originating from neighboring

622 excitatory cell types such as narrow-field (NF) and wide-field (WF) cells has shown to be rare (Gale
623 and Murphy, 2018). Next-generation *in vitro* multi-neuron patch-clamp recordings (Campagnola et
624 al., 2022) could reveal important new insights into the cell-type specific (Ayupe et al., 2023)
625 intracollicular wiring.
626 4) In addition, collicular neurons in the visual layers also get inputs from deeper SC layers. However,
627 excitatory connections from deep SC to the upper layers are rather uncommon (Gale and Murphy,
628 2018; Ghitani et al., 2014). Despite these studies have highlighted different sources of excitation
629 onto inhibitory SC neurons, further studies are required that elucidate the role and strength of input
630 that deep SC layers or external sources provide to drive inhibitory SC populations.
631
632 In this study, we recorded populations of well-isolated single units including RGCs as well as
633 GABAergic and non-GABAergic SC neurons in VGAT-ChR2 mice *in vivo*. Our approach using
634 VGAT-ChR2 mice to target all types of inhibitory SC neurons that express the vesicular GABA
635 transporter VGAT enables a first impression on how inhibitory neurons sculpt retinocollicular
636 signaling. Our inhibitory population is made up of 30% of the recorded SC neurons and connected
637 pairs. These observations are in line with previous findings showing that in the upper SC layers, a
638 substantial part of neurons (30%) are GABAergic (Ranney Mize, 1992; Whyland et al., 2020) and
639 that around one third of the postsynaptic targets of retinocollicular terminals are GABAergic (Boka
640 et al., 2006; Whyland et al., 2020).
641
642 In the last decade, the diversity of SC cell types has been mainly characterized based on morphology
643 and response properties (Franceschi and Solomon, 2018; Ito et al., 2017). Morphologically and
644 functionally, four distinct classes of retinorecipient SC neurons have been identified: stellate,
645 horizontal, wide-field and narrow field neurons (Gale and Murphy, 2016, 2014). Excitatory SC cell
646 types such as wide-field, stellate and narrow-field cells differ in morphological characteristics. This
647 morphological diversity might also be linked to how these cells integrate inputs from the retina.
648 Smaller cells, such as narrow-field (NF) and stellate cells, typically have smaller RF sizes. Their
649 limited dendritic arborization enables them to selectively respond to specific visual features. NF
650 neurons show strong direction selectivity (DS) suggesting that these cells might be strongly driven
651 by the retina, likely from DS-RGCs (Gale and Murphy, 2014). In contrast, wide-field cells have
652 extensive dendritic arbors and large RF sizes. These cells likely integrate inputs from multiple RGC
653 axons (Gale and Murphy, 2014).
654
655 The use of genetic mouse lines provides a valuable tool for understanding the circuitry and functional
656 roles of different neuron classes by selectively targeting specific cell types. Advanced techniques
657 have started to shed light on this diversity by providing cell-type characterizations on the molecular
658 level (Barchini et al., 2018; Gale and Murphy, 2018, 2014; Li and Meister, 2022; Villalobos et al.,

2018). Three categories of potential GABAergic interneurons have been classified in the SC by the use of Cre-lines (Whyland et al., 2020) that can be further subdivided into intrinsic interneurons and potential projection neurons. A recent study by Tsai et al. (2022) has mapped retinocollicular connectivity by targeting specific RGC-SC circuits using a novel approach (Trans-Seq) to classify subsets of SC cell-types that are innervated by genetically defined RGC types (Tsai et al., 2022). They identified five inhibitory clusters of retinorecipient SC cells that allow to specifically map retinocollicular connectivity. In addition, 12 distinct inhibitory subtypes across the entire SC circuit have been recently identified using single-nucleus RNA sequencing (Ayupe et al., 2023). Thus, we are at an enthralling stage where information on SC cell-types finally becomes available based on gene expression patterns, alike to the cortical circuit (Tremblay et al., 2016). Likewise investigating how optogenetic manipulation of SC INs modulates functional properties of recorded SC EXNs (Gale and Murphy, 2016) is crucial for gaining a mechanistic understanding of visual processing within the SC circuitry. Hence, a key step forward would be to leverage the tracing and transcriptomics studies and combine these methods with our high-density recording approach to enable a finer characterization of the collicular interneuron diversity and the complexity of their connectivity patterns *in vivo*.

Taken together, our study targeted a heterogeneous population of GABAergic neurons in VGAT-ChR2 mice and our results reveal that excitatory and inhibitory neurons in the two main brain areas for visual processing, the visual cortex and the superior colliculus, integrate sensory afferent inputs in different ways.

ACKNOWLEDGEMENTS

We thank J. Poulet for providing us the VGAT-ChR2 mice; KL. Teh, T. Lupashina and J. Kosubek-Langer for comments on the manuscript. We thank the Neuropixels community for their support. This work was supported by the DFG Emmy-Noether grants KR 4062/4–1 and KR 4062/4–2 (JK).

AUTHOR CONTRIBUTIONS

C.G. and J.K. conceived and designed the study; C.G. collected the data; C.G., J.S., and J.K. analyzed the data and C.G. and J.K. wrote the manuscript with inputs from J.S..

DECLARATION OF INTERESTS

The authors declare no competing interests.

MATERIALS AND METHODS

Experimental Design

Animals

All experiments were carried out in accordance with the guidelines given by Landesamt für Gesundheit und Soziales (LAGeSo - G 0142/18) Berlin and were approved by the authority. Adult VGAT-ChR2 (Slc32a1-COP4∗H134R/EYFP, The Jackson Laboratory, stock no. 014548, n= 9) transgenic mice of either sex were used to activate inhibitory neurons (Zhao et al., 2011). Mice were aged 7-9 months old on the day of recordings.

Surgical procedures

All experiments were conducted in VGAT-ChR2 mice of both sexes. Mice were induced with 2.0-2.5% isoflurane (CP-Pharma) in an induction chamber and transferred to the surgery. Once anesthetized, the surgery was performed in a stereotactic frame (Narishige) with a closed-loop temperature controller (FHC DC) for monitoring the animal's body temperature and maintaining it at 37°C. The isoflurane level was gradually lowered during surgery and maintained at 0.8-1.5% while ensuring a complete absence of vibrissa twitching or responses to tactile stimulation. During surgery, the eyes were protected with eye ointment (Vidisic, Bausch+Lomb). Mice were head-fixed in the frame, and the skull was exposed. The head was aligned along the anterior-posterior axis and marks were made for the craniotomy at 600-1500 µm ML and 0-1500 µm AP from Lambda (Paxinos and Franklin, Nixdorf 2007 stereotactic atlas) using a micromanipulator (Luigs and Neumann). For optotagging experiments, an additional mark for the optic fiber placement was made at 3500 µm AP, 500-1200 µm ML to Bregma. A headpost was placed on the skull and implanted with dental cement (Paladur). Dental cement was also used to build a recording chamber to provide a bath for grounding. During this step, a silver wire (AG-10W, Science Products) was attached to the dental cement chamber for grounding. It is important to keep the dental cement chamber low enough on the anterior and posterior sides to allow for the shallow angle probe and fiber implantations, see Sibille et al (2022) for a detailed description of the method (Sibille et al., 2022b). Craniotomies were made at the marked positions using a dental drill (Johnson-Promident). To allow for the probe insertion at a horizontal angle between 15° and 20°, a small part of the skull at the posterior part of the craniotomy was slightly thinned using the drill to ensure a smooth insertion (Sibille et al., 2022b).

Anesthetized extracellular recordings and optogenetic stimulation

Electrophysiological recordings in SC were performed in 9 anesthetized mice of both sexes (4 female, 5 male) using Neuropixels 1.0 probes (Jun et al., 2017). Data were acquired at a sampling rate of 30 kHz using the Open Ephys acquisition software and GUI (Siegle et al., 2017) (www.open-ephys.org) and the PXIe hardware acquisition system (National Instrument NI-PXIe-1071). The signal was amplified and stored in both the local field potential band (LFP, high pass-filtered 0-300

Hz) and the action potential band (AP, 300 Hz to 3 kHz). The tangential recordings along the anterior-posterior axis in SC were performed as described in Sibille et al. (2022) (Sibille et al., 2022a). The fiber for optogenetic stimulation was inserted in the SC prior to the Neuropixels probe implantation to decrease mechanical pressure and reduce drift of the electrode probe. The angled optogenetic fiber was zeroed at the brain surface and inserted from the anterior in a 60-70° angle towards the AP axis (see Figure 1A) and slowly lowered using a manual micromanipulator until reaching an insertion of 150-200 µm. Following the fiber implantation, the Neuropixels probe was inserted tangentially in a 15 to 20° angle in the superior colliculus (SC) using a micromanipulator (NewScale). The probe was zeroed at Lambda and inserted 500-1200 µm ML and 2800-3800 µm DV. After the Neuropixels probe was implanted, the optic fiber was lowered further slowly (to a maximum insertion depth of ~250 µm) and LED pulses were applied to test for optogenetic activation of cells. After correct placement, the probe and fiber were allowed to settle for 15-20 minutes before data acquisition was started. In addition, confirmation of probe placement within the SC was done via receptive field (RF) mapping to check the number of channels with RFs. RFs were estimated from the multi-unit activity (MUA) using spike-triggered average (STA) (Sibille et al., 2022b) (Figure 1C).

Optotagging to identify GABAergic neurons in VGAT-ChR2 mice

We identified ("optotagged") populations of single GABAergic SC neurons via Channelrhodopsin-2 (ChR2) activation in VGAT-ChR2 mice. The optic fiber was calibrated prior to each experiment to ensure a stable light output (2.5mW) measured at the fiber tip. Before the electrode probe insertion (see above), the optic fiber (NA .66, 200 µm core diameter, with a bare fiber tip, PlexBright, Plexon) coupled to a blue (470 nm) LED module (PlexBright, Plexon) was inserted using a 60-70° angle tilted towards the AP axis (Figure 1A). Blue light pulses were used to evoke spiking activity in VGAT-expressing neurons and to verify the proper alignment of the optic fiber and the Neuropixels probe. If no optogenetically evoked neuronal activity was observed, either the fiber was lowered to a maximum of 250 µm or the probe position was re-adjusted to ensure both the activation and recording of GABAergic SC neurons. Once the Neuropixels electrode probe and optic fiber were properly aligned, optogentic stimulation using either a square wave or Gaussian function stimulus pulse was applied to identify light-activated channels (Figure 1A, B). As the stimulation using a square wave pulse led to the induction of light artefacts in the spiking response (Jun et al., 2017), we manually removed these artefacts in a post-processing step by interpolating the raw values in each channel during the onset and offset of the square pulse in 2 out of 11 experiments. In order to decrease light artefacts induced by the sharp light onset in the square wave pulse, we changed the pulse to using a Gaussian function stimulus pulse to gradually increase light intensity in the remaining 8 experiments. The light pulses were applied during spontaneous conditions (presentation of a black background, 100 ms pulse duration, 2 Hz, 200 trials, 2.7- 3.5 mW measured at the fiber tip) and conditions with visually evoked activity (checkerboard stimulus, 1000 ms pulse duration, 30

trials ON, 30 trials OFF, 2.7- 3.5 mW measured at the fiber tip, n = 10/11 experiments). Both stimulation protocols were shown twice within the recording to ensure stable responses throughout the recording session. GABAergic neurons were identified by their increased short-latency responses to blue light stimulation pulses. When we compared the visually evoked responses to those induced by ChR2 activation we found that they varied in their temporal activation profile (Figure 1B, C). The response to the visual sparse noise stimulus starts ~80ms after the stimulus onset (Figure 1C) while responses induced by ChR2 activation had a shorter latency following light onset (Figure 1C).

Visual stimulation

Visual stimuli were generated in Python using the PsychoPy2 toolbox (Peirce et al., 2019). The visual stimuli were displayed on a calibrated screen (Dell, refresh rate = 120 Hz, mean luminance = 120 cd/m²). For receptive field mapping, we presented the sparse noise visual stimulus on a grid of 24x 14 squares. The sparse noise targets were either dark (on light background) or light (on dark background) and 10 deg in size with [n_targets per frame, n_trials per position] = [2,20] and presented for 100 ms. A set of standardized different visual stimuli was presented including a natural movie (30 trials, randomized with other stimuli, 10s) taken from Froudarakis et al. (2014) (Froudarakis et al., 2014) and a full-field chirp stimulus (Baden et al., 2016). The frametimes of the visual stimuli were marked by stimulus-locked synchronizing events (TTLs).

Histology

For histological reconstruction of the electrode track, the probe was removed, coated with fluorescent dye (DiI, Abcam-ab145311) and re-inserted in the same location. In a few experiments we performed multiple recordings and only stained the last insertion. Subsequently, the animal was terminated with an excess of isoflurane (> 4%). Cardiac perfusion was performed with phosphate buffer saline (PBS) followed by 4% paraformaldehyde (PFA) in PBS. Brains were post-fixed overnight in 4% PFA, and stored in PBS until slicing (100 µm) on a vibratome (Leica VT1000S). The brain slices were mounted using a mounting medium containing DAPI (DAPI-Flouromount-G, Biozol Cat. 0100-20). Slices were imaged on a fluorescence microscope using a 2.5 x objective for post hoc visualization of the electrode probe track.

Data analysis and statistical analyses

Data analysis was performed in Python 3 .0 (www.anaconda.com) using custom-written scripts. MATLAB 2019b (www.mathworks.com) was used for spike sorting, see below. Statistical tests were performed using the two-sided Wilcoxon rank-sum test for unpaired samples and the Wilcoxon signed-rank test (two-sided) for paired samples using the scipy.stats module in Python, unless stated otherwise. For correlation analyses we used Pearson correlation implemented via the linregress

808 function. Population results are indicated as mean ± standard deviation if not stated otherwise. The
809 number of neurons and animals used in each analysis is reported in the Results section or figure
810 legends.
811
812 Multi-unit activity extraction
813 For MUA analysis, common average referencing was applied to the bandpass filtered AP data
814 (Butterworth filter order 2, 0.3 to 3 kHz), where each event is extracted using custom-written Python
815 scripts. Spike detection was performed for each channel independently at a threshold of 4 standard
816 deviations in the AP band (double side detection). The scripts for performing the MUA analysis are
817 available on the GitHub repository (https://github.com/KremkowLab/tangential_recording)
818
819 Offline Spike sorting and criteria for unit classification
820 KiloSort2 and 3 (Pachitariu et al., 2016) (https://github.com/MouseLand/Kilosort) were used for
821 automatic detection and clustering of spikes followed by manual curation using phy2 (Rossant et al.,
822 2016) (https://github.com/cortex-lab/phy). Double-counted spikes were removed for each cluster
823 (within ± 0.16 ms) (Siegle et al., 2021). Furthermore, clusters with between-unit overlapping spikes
824 that show above chance zero-lag peaks in the cross-correlograms (CCG, peak windows ± 0.5 ms)
825 were re-evaluated individually in phy to be either refined or removed. Inter-spike-interval (ISI)
826 violations were calculated as the ratio of the spikes within the refractory period (± 1.5 ms) to the total
827 number of spikes. Units with ISI > 0.05% were removed. We also checked for stable firing of clusters
828 throughout the recording. Furthermore, we excluded units from further analysis that were lying
829 outside the optogenetic stimulation range (see below, Identification of Inhibitory neurons, see Figure
830 1B) and outside the SC boundaries (from STA RFs on MUA, see Figure 1C).
831
832 Waveform classification to identify RGC axons and SC neurons
833 A waveform classification approach was applied to distinguish action potentials (APs) from retinal
834 ganglion cell (RGC) axons and somatic APs from SC neurons (Sibille et al., 2022a). In brief, we
835 calculated the multi-channel waveform (MCW) which reflects the spatiotemporal profile of the AP
836 signals. Afferent axons and somatic signals could be classified based on their distinct waveform
837 which allowed us to classify clusters into afferent axon AP vs somatic AP. In essence, due to the SC
838 electrode probe implantation along the anterior-posterior (AP) axis, the electrode captures signals
839 from retinal axons that innervate the SC along the electrode channels. This propagation of RGC
840 axonal action potentials along the axonal path is visible in the spatiotemporal profile of their multi-
841 channel waveforms (Figure 1D, left).
842
843
844

Waveform classification approach to separate GABAergic and non-GABAergic SC neurons

We performed standard waveform analyses to attempt to separate GABAergic SC neurons based on waveform features (Jia et al., 2019; Quirk et al., 2009) (Figure 1 – figure supplement 2). Briefly, we detected the negative (trough) and positive peak (peak) from single-channel waveforms and calculated their peak-to-trough duration. The amplitude was defined as the absolute difference between trough and peak. The peak-to-trough ratio was defined as the ratio between amplitudes of peak and trough.

Post hoc separation of GABAergic and non-GABAergic SC neurons

To study retinal input integration in a cell-type specific manner, we used a method to separate the neural responses of GABAergic neurons from that of excitatory neurons in the SC. First, we identified the minimum and maximum recording sites on the probe that were photo-activated. These borders were defined via the minimum and maximum peak channel of light-induced units that are activated on the probe. SC neurons that did not fall inside this optogenetic stimulation range (identified by their peak channel) were excluded from further analysis. We employed stringent criteria for determining the boundaries of LED evoked response and selection of neurons to be included (Figure 1 – figure supplement 1). The distribution of excitatory and inhibitory SC neurons is not significantly different for 9/11 experiments (Wilcoxon rank-sum, p values = 0.307, 0.0115, 0.7.55, 0.834, 5.01×10^{-6}, 0.79, 0.80, 0.26, 0.33, 0.08, 0.13). In the two significantly different experiments only 2 RGC-SC EXN pairs were located in the region without identified SC INs, and thus will not affect the results. SC neurons were separated based on their short-latency increase in responses to blue light pulses during two different protocols: (1) baseline activity (black background, 100 ms pulse duration, 2 Hz pulse frequency) and (2) during a checkerboard stimulus (1000 ms pulse duration, 30 trials LED ON, 30 trials LED OFF). This classification was done using a custom-written graphical-user-interface (GUI) approach where units were labeled as either “light-responsive”, “non light-responsive”. The labeling step was conducted by three independent observers. A unit was included if 2 out of 3 observers chose the same label. Units with unstable firing throughout the recording period were excluded from further analysis.

Identification of synaptically connected RGC-SC pairs

Monosynaptic connections between RGC axons and SC neurons were detected using established methods (Bereshpolova et al., 2020; Clay Reid and Alonso, 1995; Denman and Contreras, 2015; Usrey et al., 1998) based on statistically significant peaks at synaptic delays. Briefly, we calculated a jittered (timescale jitter 5 ms) version of each spike train by randomizing all spike times within a consecutive 10-15 ms window (Smith and Kohn, 2008). We then calculated the cross-correlation between a pair of neurons both for the original (raw CCG) and the jittered spike train (jittered CCG). Subtracting the jittered CCG from the raw CCG results in a jitter-corrected version of the CCG which

was used for monosynaptic pairs detection. Connected pairs were identified using cross-correlation analysis and significant peaks (peak detection window from + 0.5 to 3.5 ms) had to extend over the threshold (baseline + 4x standard deviation) for at least 5 consecutive time bins (0.1 ms resolution) (as described previously, in Sibille et al. (2022) (Sibille et al., 2022a). The cross-correlations were calculated using the Python pycorrelate package (https://github.com/tritemio/pycorrelate). Please note that for CCG analysis, spike trains were correlated over the full recording duration, except for periods with optogenetic stimulation. Latencies to peak response were calculated from the CCGs as the maximum time within the response window.

Analysis of retinocollicular connection strength

Synaptic efficacy and contribution measures of connected RGC-SC pairs were estimated from spiketrains during the entire recording session (except for optotagging periods which were excluded) using standard approaches (Bereshpolova et al., 2020; Clay Reid and Alonso, 1995; Swadlow and Gusev, 2002; Usrey et al., 1998). Briefly, efficacy was estimated from the baseline-corrected CCGs by dividing the area of the CCG peak (baseline window: > -1 to < 0.4 ms, peak window: >0.4 to <3.5 ms) by the total number of presynaptic spikes. Thus, an efficacy measure of 1 (100%) would reflect that for each presynaptic retinal spike, a postsynaptic spike could be detected. To estimate the connection contribution, we counted the number of SC spikes that were preceded by a retinal afferent spike, integrated over a time window between -3 to -0.5 ms, and divided this number by the total number of SC spikes. A contribution of 1 (100%) indicates that all spikes of an SC neuron are preceded by retinal afferent spikes.

Paired-spike dynamics analysis

For estimation of paired-spike dynamics, baseline-corrected CCGs were re-calculated triggered on 1st and 2nd RGCs using the same baseline and peak windows as mentioned above. We identified pairs of retinal spikes (1st and 2nd RGC) for each RGC-SC connected pair (Usrey et al., 1998). Briefly, a pair of retinal spikes was defined by a specific inter-spike interval (ISI) where the second RGC spike followed the 1st RGC by a ISI of 5 to 30 ms. The second criterion for classifying a pair of retinal spikes was a certain dead time where the 1st retinal spike was preceded by a minimum period of silence (dead time: 30ms). The dead time criterion was applied to ensure a comparable level of activity immediately preceding all first spikes. The preceding window (> -1 to < 0.4 ms) was used as a baseline window. Paired-spike enhancement was calculated as the ratio of efficacy for the 2nd RGC to the efficacy for the 1st RGC.

Functional similarity analysis of retinocollicular connected pairs

To characterize the functional similarity between connected RGCs and the target neurons in the SC, we estimated the functional similarity index. To do so, we calculated the correlation coefficients from

responses during the light and dark sparse noise (r_{SL} and r_{SD}) as well as during the natural movie stimulus (r_{NM}), phase scrambled movie (r_{PSM}) and during a checkerboard stimulus (r_{Chk}). The similarity index was calculated between the responses of the RGC and the responses of the postsynaptic SC neuron. As a result, the similarity index reflects the degree of similarity in the responses of the connected pairs. The correlation of activity during sparse noise stimuli (r_{SL} and r_{SD}) was estimated from the spatiotemporal receptive fields (STRFs) which were calculated from the STA. The similarity during the other stimuli (r_{NM}, r_{PSM} and r_{Chk}) were calculated from the PSTHs. We limited this analysis step to neurons with high signal-to-noise ratio (SNR) in the visually evoked activity (SNR > 8 for the STRFs). The overall similarity index was then calculated from the averaged correlation coefficients functional similarity index = $(r_{SD} + r_{SL} + r_{NM} + r_{PSM} + r_{Chk})/5$.

Data availability

The datasets that support the findings of this study are available from the corresponding author on request.

Code availability

Custom Python code is available from the corresponding author on request.

REFERENCES

Agmon A, Connors BW. 1992. Correlation between intrinsic firing patterns and thalamocortical synaptic responses of neurons in mouse barrel cortex. *J Neurosci Off J Soc Neurosci* **12**:319–329. doi:10.1523/JNEUROSCI.12-01-00319.1992

Alonso J-M, Swadlow HA. 2005. Thalamocortical specificity and the synthesis of sensory cortical receptive fields. *J Neurophysiol* **94**:26–32. doi:10.1152/jn.01281.2004

Alonso J-M, Usrey WM, Reid RC. 2001. Rules of Connectivity between Geniculate Cells and Simple Cells in Cat Primary Visual Cortex. *J Neurosci* **21**:4002–4015. doi:10.1523/JNEUROSCI.21-11-04002.2001

Alonso JM, Usrey WM, Reid RC. 1996. Precisely correlated firing in cells of the lateral geniculate nucleus. *Nature* **383**:815–819. doi:10.1038/383815a0

Ayupe AC, Choi JS, Beckedorff F, Mccartan R, Levay K, Park KK. 2023. Single-Nucleus RNA Sequencing of Developing and Mature Superior Colliculus Identifies Neuronal Diversity and Candidate Mediators of Circuit Assembly. *BioRxiv Prepr Serv Biol* 2023.02.01.526254. doi:10.1101/2023.02.01.526254

Baden T, Berens P, Franke K, Román Rosón M, Bethge M, Euler T. 2016. The functional diversity of retinal ganglion cells in the mouse. *Nature* **529**:345–350. doi:10.1038/nature16468

Barchini J, Shi X, Chen H, Cang J. 2018. Bidirectional encoding of motion contrast in the mouse superior colliculus. *eLife* **7**:e35261. doi:10.7554/eLife.35261

Bereshpolova Y, Hei X, Alonso J-M, Swadlow HA. 2020. Three rules govern thalamocortical connectivity of fast-spike inhibitory interneurons in the visual cortex. *eLife* **9**:e60102. doi:10.7554/eLife.60102

965 Bereshpolova Y, Stoelzel CR, Gusev AG, Bezdudnaya T, Swadlow HA. 2006. The impact of a
966 corticotectal impulse on the awake superior colliculus. *J Neurosci Off J Soc Neurosci*
967 **26**:2250–2259. doi:10.1523/JNEUROSCI.4402-05.2006
968 Boka K, Chomsung R, Li J, Bickford ME. 2006. Comparison of the ultrastructure of cortical and
969 retinal terminals in the rat superior colliculus. *Anat Rec A Discov Mol Cell Evol Biol*
970 **288A**:850–858. doi:10.1002/ar.a.20359
971 Bruno RM, Sakmann B. 2006. Cortex is driven by weak but synchronously active thalamocortical
972 synapses. *Science* **312**:1622–1627. doi:10.1126/science.1124593
973 Bruno RM, Simons DJ. 2002. Feedforward Mechanisms of Excitatory and Inhibitory Cortical
974 Receptive Fields. *J Neurosci* **22**:10966–10975. doi:10.1523/JNEUROSCI.22-24-
975 10966.2002
976 Butler AB. 2008. Evolution of the thalamus: a morphological and functional review. *Thalamus Relat*
977 *Syst* **4**:35–58. doi:10.1017/S1472928808000356
978 Campagnola L, Seeman SC, Chartrand T, Kim L, Hoggarth A, Gamlin C, Ito S, Trinh J, Davoudian
979 P, Radaelli C, Kim M-H, Hage T, Braun T, Alfiler L, Andrade J, Bohn P, Dalley R, Henry A,
980 Kebede S, Alice M, Sandman D, Williams G, Larsen R, Teeter C, Daigle TL, Berry K,
981 Dotson N, Enstrom R, Gorham M, Hupp M, Dingman Lee S, Ngo K, Nicovich PR,
982 Potekhina L, Ransford S, Gary A, Goldy J, McMillen D, Pham T, Tieu M, Siverts L, Walker
983 M, Farrell C, Schroedter M, Slaughterbeck C, Cobb C, Ellenbogen R, Gwinn RP, Keene
984 CD, Ko AL, Ojemann JG, Silbergeld DL, Carey D, Casper T, Crichton K, Clark M, Dee N,
985 Ellingwood L, Gloe J, Kroll M, Sulc J, Tung H, Wadhwani K, Brouner K, Egdorf T, Maxwell
986 M, McGraw M, Pom CA, Ruiz A, Bomben J, Feng D, Hejazinia N, Shi S, Szafer A,
987 Wakeman W, Phillips J, Bernard A, Esposito L, D'Orazi FD, Sunkin S, Smith K, Tasic B,
988 Arkhipov A, Sorensen S, Lein E, Koch C, Murphy G, Zeng H, Jarsky T. 2022. Local
989 connectivity and synaptic dynamics in mouse and human neocortex. *Science*
990 **375**:eabj5861. doi:10.1126/science.abj5861
991 Carter DA, Aguayo AJ, Bray GM. 1991. Retinal ganglion cell terminals in the hamster superior
992 colliculus: An ultrastructural study. *J Comp Neurol* **311**:97–107.
993 doi:10.1002/cne.903110108
994 Chandrasekaran AR, Shah RD, Crair MC. 2007. Developmental Homeostasis of Mouse
995 Retinocollicular Synapses. *J Neurosci* **27**:1746–1755. doi:10.1523/JNEUROSCI.4383-
996 06.2007
997 Clay Reid R, Alonso J-M. 1995. Specificity of monosynaptic connections from thalamus to visual
998 cortex. *Nature* **378**:281–284. doi:10.1038/378281a0
999 Cruikshank SJ, Lewis TJ, Connors BW. 2007. Synaptic basis for intense thalamocortical activation
1000 of feedforward inhibitory cells in neocortex. *Nat Neurosci* **10**:462–468. doi:10.1038/nn1861
1001 Denman DJ, Contreras D. 2015. Complex Effects on In Vivo Visual Responses by Specific
1002 Projections from Mouse Cortical Layer 6 to Dorsal Lateral Geniculate Nucleus. *J Neurosci*
1003 **35**:9265–9280. doi:10.1523/JNEUROSCI.0027-15.2015
1004 Drager UC, Hubel DH. 1976. Topography of visual and somatosensory projections to mouse
1005 superior colliculus. *J Neurophysiol* **39**:91–101. doi:10.1152/jn.1976.39.1.91
1006 Ellis EM, Gauvain G, Sivyer B, Murphy GJ. 2016. Shared and distinct retinal input to the mouse
1007 superior colliculus and dorsal lateral geniculate nucleus. *J Neurophysiol* **116**:602–610.
1008 doi:10.1152/jn.00227.2016
1009 Essig J, Hunt JB, Felsen G. 2021. Inhibitory neurons in the superior colliculus mediate selection of
1010 spatially-directed movements. *Commun Biol* **4**:719. doi:10.1038/s42003-021-02248-1
1011 Evangelio M, García-Amado M, Clascá F. 2018. Thalamocortical Projection Neuron and
1012 Interneuron Numbers in the Visual Thalamic Nuclei of the Adult C57BL/6 Mouse. *Front*
1013 *Neuroanat* **12**.
1014 Evans DA, Stempel AV, Vale R, Ruehle S, Lefler Y, Branco T. 2018. A synaptic threshold
1015 mechanism for computing escape decisions. *Nature* **558**:590–594. doi:10.1038/s41586-
1016 018-0244-6
1017 Ferrarese L, Jouhanneau J-S, Remme MWH, Kremkow J, Katona G, Rózsa B, Schreiber S, Poulet
1018 JFA. 2018. Dendrite-Specific Amplification of Weak Synaptic Input during Network Activity
1019 In Vivo. *Cell Rep* **24**:3455-3465.e5. doi:10.1016/j.celrep.2018.08.088

Franceschi G, Solomon SG. 2018. Visual response properties of neurons in the superficial layers of the superior colliculus of awake mouse. *J Physiol* **596**:6307–6332. doi:10.1113/JP276964

Froudarakis E, Berens P, Ecker AS, Cotton RJ, Sinz FH, Yatsenko D, Saggau P, Bethge M, Tolias AS. 2014. Population code in mouse V1 facilitates readout of natural scenes through increased sparseness. *Nat Neurosci* **17**:851–857. doi:10.1038/nn.3707

Furman M, Xu H-P, Crair MC. 2013. Competition driven by retinal waves promotes morphological and functional synaptic development of neurons in the superior colliculus. *J Neurophysiol* **110**:1441–1454. doi:10.1152/jn.01066.2012

Gabernet L, Jadhav SP, Feldman DE, Carandini M, Scanziani M. 2005. Somatosensory integration controlled by dynamic thalamocortical feed-forward inhibition. *Neuron* **48**:315–327. doi:10.1016/j.neuron.2005.09.022

Gale SD, Murphy GJ. 2018. Distinct cell types in the superficial superior colliculus project to the dorsal lateral geniculate and lateral posterior thalamic nuclei. *J Neurophysiol* **120**:1286–1292. doi:10.1152/jn.00248.2018

Gale SD, Murphy GJ. 2016. Active Dendritic Properties and Local Inhibitory Input Enable Selectivity for Object Motion in Mouse Superior Colliculus Neurons. *J Neurosci* **36**:9111–9123. doi:10.1523/JNEUROSCI.0645-16.2016

Gale SD, Murphy GJ. 2014. Distinct representation and distribution of visual information by specific cell types in mouse superficial superior colliculus. *J Neurosci Off J Soc Neurosci* **34**:13458–13471. doi:10.1523/JNEUROSCI.2768-14.2014

Ghitani N, Bayguinov PO, Vokoun CR, McMahon S, Jackson MB, Basso MA. 2014. Excitatory Synaptic Feedback from the Motor Layer to the Sensory Layers of the Superior Colliculus. *J Neurosci* **34**:6822–6833. doi:10.1523/JNEUROSCI.3137-13.2014

Gibson JR, Beierlein M, Connors BW. 1999. Two networks of electrically coupled inhibitory neurons in neocortex. *Nature* **402**:75–79. doi:10.1038/47035

Glickfeld LL, Histed MH, Maunsell JHR. 2013. Mouse Primary Visual Cortex Is Used to Detect Both Orientation and Contrast Changes. *J Neurosci* **33**:19416–19422. doi:10.1523/JNEUROSCI.3560-13.2013

Hoy JL, Bishop HI, Niell CM. 2019. Defined Cell Types in Superior Colliculus Make Distinct Contributions to Prey Capture Behavior in the Mouse. *Curr Biol* **29**:4130-4138.e5. doi:10.1016/j.cub.2019.10.017

Huberman AD, Manu M, Koch SM, Susman MW, Lutz AB, Ullian EM, Baccus SA, Barres BA. 2008. Architecture and Activity-Mediated Refinement of Axonal Projections from a Mosaic of Genetically Identified Retinal Ganglion Cells. *Neuron* **59**:425–438. doi:10.1016/j.neuron.2008.07.018

Inayat S, Barchini J, Chen H, Feng L, Liu X, Cang J. 2015. Neurons in the Most Superficial Lamina of the Mouse Superior Colliculus Are Highly Selective for Stimulus Direction. *J Neurosci* **35**:7992–8003. doi:10.1523/JNEUROSCI.0173-15.2015

Inoue T, Imoto K. 2006. Feedforward inhibitory connections from multiple thalamic cells to multiple regular-spiking cells in layer 4 of the somatosensory cortex. *J Neurophysiol* **96**:1746–1754. doi:10.1152/jn.00301.2006

Isaacson JS, Scanziani M. 2011. How Inhibition Shapes Cortical Activity. *Neuron* **72**:231–243. doi:10.1016/j.neuron.2011.09.027

Ito S, Feldheim DA, Litke AM. 2017. Segregation of Visual Response Properties in the Mouse Superior Colliculus and Their Modulation during Locomotion. *J Neurosci* **37**:8428–8443. doi:10.1523/JNEUROSCI.3689-16.2017

Ji X, Zingg B, Mesik L, Xiao Z, Zhang LI, Tao HW. 2016. Thalamocortical Innervation Pattern in Mouse Auditory and Visual Cortex: Laminar and Cell-Type Specificity. *Cereb Cortex* **26**:2612–2625. doi:10.1093/cercor/bhv099

Jia X, Siegle JH, Bennett C, Gale SD, Denman DJ, Koch C, Olsen SR. 2019. High-density extracellular probes reveal dendritic backpropagation and facilitate neuron classification. *J Neurophysiol* **121**:1831–1847. doi:10.1152/jn.00680.2018

Jin J, Wang Y, Swadlow HA, Alonso JM. 2011. Population receptive fields of ON and OFF thalamic inputs to an orientation column in visual cortex. *Nat Neurosci* **14**:232–238. doi:10.1038/nn.2729

Jouhanneau J-S, Kremkow J, Poulet JFA. 2018. Single synaptic inputs drive high-precision action potentials in parvalbumin expressing GABA-ergic cortical neurons in vivo. *Nat Commun* **9**:1540. doi:10.1038/s41467-018-03995-2

Jun JJ, Steinmetz NA, Siegle JH, Denman DJ, Bauza M, Barbarits B, Lee AK, Anastassiou CA, Andrei A, Aydın Ç, Barbic M, Blanche TJ, Bonin V, Couto J, Dutta B, Gratiy SL, Gutnisky DA, Häusser M, Karsh B, Ledochowitsch P, Lopez CM, Mitelut C, Musa S, Okun M, Pachitariu M, Putzeys J, Rich PD, Rossant C, Sun W, Svoboda K, Carandini M, Harris KD, Koch C, O'Keefe J, Harris TD. 2017. Fully integrated silicon probes for high-density recording of neural activity. *Nature* **551**:232–236. doi:10.1038/nature24636

Kaneda K, Isa K, Yanagawa Y, Isa T. 2008. Nigral Inhibition of GABAergic Neurons in Mouse Superior Colliculus. *J Neurosci* **28**:11071–11078. doi:10.1523/JNEUROSCI.3263-08.2008

Kara P, Reid RC. 2003. Efficacy of Retinal Spikes in Driving Cortical Responses. *J Neurosci* **23**:8547–8557. doi:10.1523/JNEUROSCI.23-24-08547.2003

Kasai M, Isa T. 2016. Imaging population dynamics of surround suppression in the superior colliculus. *Eur J Neurosci* **44**:2543–2556. doi:10.1111/ejn.13371

Kremkow J, Aertsen A, Kumar A. 2010a. Gating of Signal Propagation in Spiking Neural Networks by Balanced and Correlated Excitation and Inhibition. *J Neurosci* **30**:15760–15768. doi:10.1523/JNEUROSCI.3874-10.2010

Kremkow J, Alonso J-M. 2018. Thalamocortical Circuits and Functional Architecture. *Annu Rev Vis Sci* **4**:263–285. doi:10.1146/annurev-vision-091517-034122

Kremkow J, Perrinet LU, Masson GS, Aertsen A. 2010b. Functional consequences of correlated excitatory and inhibitory conductances in cortical networks. *J Comput Neurosci* **28**:579–594. doi:10.1007/s10827-010-0240-9

Kremkow J, Perrinet LU, Monier C, Alonso J-M, Aertsen A, Frégnac Y, Masson GS. 2016. Push-Pull Receptive Field Organization and Synaptic Depression: Mechanisms for Reliably Encoding Naturalistic Stimuli in V1. *Front Neural Circuits* **10**.

Kyriazi HT, Carvell GE, Simons DJ. 1994. OFF response transformations in the whisker/barrel system. *J Neurophysiol* **72**:392–401. doi:10.1152/jn.1994.72.1.392

Lashley KS. 1931. The mechanism of vision IV. The cerebral areas necessary for pattern vision in the rat. *J Comp Neurol* **53**:419–478. doi:10.1002/cne.900530304

Lee CM, Osman AF, Volgushev M, Escabí MA, Read HL. 2016. Neural spike-timing patterns vary with sound shape and periodicity in three auditory cortical fields. *J Neurophysiol* **115**:1886–1904. doi:10.1152/jn.00784.2015

Lee S-H, Kwan AC, Zhang S, Phoumthipphavong V, Flannery JG, Masmanidis SC, Taniguchi H, Huang ZJ, Zhang F, Boyden ES, Deisseroth K, Dan Y. 2012. Activation of specific interneurons improves V1 feature selectivity and visual perception. *Nature* **488**:379–383. doi:10.1038/nature11312

Levick WR, Cleland BG, Dubin MW. 1972. Lateral geniculate neurons of cat: retinal inputs and physiology. *Invest Ophthalmol* **11**:302–311.

Li Y, Meister M. 2022. Functional Cell Types in the Mouse Superior Colliculus (preprint). Neuroscience. doi:10.1101/2022.04.01.486789

Lien AD, Scanziani M. 2018. Cortical direction selectivity emerges at convergence of thalamic synapses. *Nature* **558**:80–86. doi:10.1038/s41586-018-0148-5

Liu Y, Savier EL, DePiero VJ, Chen C, Schwalbe DC, Abraham-Fan R-J, Chen H, Campbell JN, Cang J. 2023. Mapping visual functions onto molecular cell types in the mouse superior colliculus. *Neuron* **111**:1876-1886.e5. doi:10.1016/j.neuron.2023.03.036

Masterson SP, Zhou N, Akers BK, Dang W, Bickford ME. 2019. Ultrastructural and optogenetic dissection of V1 corticotectal terminal synaptic properties. *J Comp Neurol* **527**:833–842. doi:10.1002/cne.24538

Mastronarde DN. 1987. Two classes of single-input X-cells in cat lateral geniculate nucleus. II. Retinal inputs and the generation of receptive-field properties. *J Neurophysiol* **57**:381–413. doi:10.1152/jn.1987.57.2.381

Miller KD. 2016. Canonical computations of cerebral cortex. *Curr Opin Neurobiol* **37**:75–84. doi:10.1016/j.conb.2016.01.008

Moore AK, Wehr M. 2013. Parvalbumin-expressing inhibitory interneurons in auditory cortex are well-tuned for frequency. *J Neurosci Off J Soc Neurosci* **33**:13713–13723. doi:10.1523/JNEUROSCI.0663-13.2013

Muellner FE, Roska B. 2023. Individual thalamic inhibitory interneurons are functionally specialized towards distinct visual features (preprint). Neuroscience. doi:10.1101/2023.03.22.533751

Niell CM, Scanziani M. 2021. How Cortical Circuits Implement Cortical Computations: Mouse Visual Cortex as a Model. *Annu Rev Neurosci* **44**:517–546. doi:10.1146/annurev-neuro-102320-085825

Niell CM, Stryker MP. 2008. Highly Selective Receptive Fields in Mouse Visual Cortex. *J Neurosci* **28**:7520–7536. doi:10.1523/JNEUROSCI.0623-08.2008

Ono M, Bishop DC, Oliver DL. 2017. Identified GABAergic and Glutamatergic Neurons in the Mouse Inferior Colliculus Share Similar Response Properties. *J Neurosci* **37**:8952–8964. doi:10.1523/JNEUROSCI.0745-17.2017

Pachitariu M, Steinmetz N, Kadir S, Carandini M, Kenneth D. H. 2016. Kilosort: realtime spike-sorting for extracellular electrophysiology with hundreds of channels (preprint). Neuroscience. doi:10.1101/061481

Peirce J, Gray JR, Simpson S, MacAskill M, Höchenberger R, Sogo H, Kastman E, Lindeløv JK. 2019. PsychoPy2: Experiments in behavior made easy. *Behav Res Methods* **51**:195–203. doi:10.3758/s13428-018-01193-y

Perge JA, Koch K, Miller R, Sterling P, Balasubramanian V. 2009. How the Optic Nerve Allocates Space, Energy Capacity, and Information. *J Neurosci* **29**:7917–7928. doi:10.1523/JNEUROSCI.5200-08.2009

Petruno SK, Clark RE, Reinagel P. 2013. Evidence that primary visual cortex is required for image, orientation, and motion discrimination by rats. *PloS One* **8**:e56543. doi:10.1371/journal.pone.0056543

Porter JT, Johnson CK, Agmon A. 2001. Diverse Types of Interneurons Generate Thalamus-Evoked Feedforward Inhibition in the Mouse Barrel Cortex. *J Neurosci* **21**:2699–2710. doi:10.1523/JNEUROSCI.21-08-02699.2001

Quirk MC, Sosulski DL, Feierstein CE, Uchida N, Mainen ZF. 2009. A Defined Network of Fast-Spiking Interneurons in Orbitofrontal Cortex: Responses to Behavioral Contingencies and Ketamine Administration. *Front Syst Neurosci* **3**:13. doi:10.3389/neuro.06.013.2009

Ranney Mize R. 1992. Chapter 11 The organization of GABAergic neurons in the mammalian superior colliculusProgress in Brain Research. Elsevier. pp. 219–248. doi:10.1016/S0079-6123(08)63616-X

Reid RC, Alonso JM. 1995. Specificity of monosynaptic connections from thalamus to visual cortex. *Nature* **378**:281–284. doi:10.1038/378281a0

Reinhard K, Li C, Do Q, Burke EG, Heynderickx S, Farrow K. 2019. A projection specific logic to sampling visual inputs in mouse superior colliculus. *eLife* **8**:e50697. doi:10.7554/eLife.50697

Rompani SB, Müllner FE, Wanner A, Zhang C, Roth CN, Yonehara K, Roska B. 2017. Different Modes of Visual Integration in the Lateral Geniculate Nucleus Revealed by Single-Cell-Initiated Transsynaptic Tracing. *Neuron* **93**:767-776.e6. doi:10.1016/j.neuron.2017.01.028

Rossant C, Kadir SN, Goodman DFM, Schulman J, Hunter MLD, Saleem AB, Grosmark A, Belluscio M, Denfield GH, Ecker AS, Tolias AS, Solomon S, Buzsaki G, Carandini M, Harris KD. 2016. Spike sorting for large, dense electrode arrays. *Nat Neurosci* **19**:634–641. doi:10.1038/nn.4268

Sanes JR, Masland RH. 2015. The types of retinal ganglion cells: current status and implications for neuronal classification. *Annu Rev Neurosci* **38**:221–246. doi:10.1146/annurev-neuro-071714-034120

Schröder S, Steinmetz NA, Krumin M, Pachitariu M, Rizzi M, Lagnado L, Harris KD, Carandini M. 2020. Arousal Modulates Retinal Output. *Neuron* **107**:487-495.e9. doi:10.1016/j.neuron.2020.04.026

Shang C, Liu A, Li D, Xie Z, Chen Z, Huang M, Li Y, Wang Y, Shen WL, Cao P. 2019. A subcortical excitatory circuit for sensory-triggered predatory hunting in mice. *Nat Neurosci* **22**:909–920. doi:10.1038/s41593-019-0405-4

Shang C, Liu Z, Chen Z, Shi Y, Wang Q, Liu S, Li D, Cao P. 2015. BRAIN CIRCUITS. A parvalbumin-positive excitatory visual pathway to trigger fear responses in mice. *Science* **348**:1472–1477. doi:10.1126/science.aaa8694

Sherman SM. 2004. Interneurons and triadic circuitry of the thalamus. *Trends Neurosci* **27**:670–675. doi:10.1016/j.tins.2004.08.003

Shi X, Barchini J, Ledesma HA, Koren D, Jin Y, Liu X, Wei W, Cang J. 2017. Retinal origin of direction selectivity in the superior colliculus. *Nat Neurosci* **20**:550–558. doi:10.1038/nn.4498

Sibille J, Gehr C, Benichov JI, Balasubramanian H, Teh KL, Lupashina T, Vallentin D, Kremkow J. 2022a. High-density electrode recordings reveal strong and specific connections between retinal ganglion cells and midbrain neurons. *Nat Commun* **13**:5218. doi:10.1038/s41467-022-32775-2

Sibille J, Gehr C, Teh KL, Kremkow J. 2022b. Tangential high-density electrode insertions allow to simultaneously measure neuronal activity across an extended region of the visual field in mouse superior colliculus. *J Neurosci Methods* **376**:109622. doi:10.1016/j.jneumeth.2022.109622

Siegle JH, Jia X, Durand S, Gale S, Bennett C, Graddis N, Heller G, Ramirez TK, Choi H, Luviano JA, Groblewski PA, Ahmed R, Arkhipov A, Bernard A, Billeh YN, Brown D, Buice MA, Cain N, Caldejon S, Casal L, Cho A, Chvilicek M, Cox TC, Dai K, Denman DJ, de Vries SEJ, Dietzman R, Esposito L, Farrell C, Feng D, Galbraith J, Garrett M, Gelfand EC, Hancock N, Harris JA, Howard R, Hu B, Hytnen R, Iyer R, Jessett E, Johnson K, Kato I, Kiggins J, Lambert S, Lecoq J, Ledochowitsch P, Lee JH, Leon A, Li Y, Liang E, Long F, Mace K, Melchior J, Millman D, Mollenkopf T, Nayan C, Ng L, Ngo K, Nguyen T, Nicovich PR, North K, Ocker GK, Ollerenshaw D, Oliver M, Pachitariu M, Perkins J, Reding M, Reid D, Robertson M, Ronellenfitch K, Seid S, Slaughterbeck C, Stoecklin M, Sullivan D, Sutton B, Swapp J, Thompson C, Turner K, Wakeman W, Whitesell JD, Williams D, Williford A, Young R, Zeng H, Naylor S, Phillips JW, Reid RC, Mihalas S, Olsen SR, Koch C. 2021. Survey of spiking in the mouse visual system reveals functional hierarchy. *Nature*. doi:10.1038/s41586-020-03171-x

Siegle JH, López AC, Patel YA, Abramov K, Ohayon S, Voigts J. 2017. Open Ephys: an open-source, plugin-based platform for multichannel electrophysiology. *J Neural Eng* **14**:045003. doi:10.1088/1741-2552/aa5eea

Simons DJ, Carvell GE. 1989. Thalamocortical response transformation in the rat vibrissa/barrel system. *J Neurophysiol* **61**:311–330. doi:10.1152/jn.1989.61.2.311

Smith MA, Kohn A. 2008. Spatial and Temporal Scales of Neuronal Correlation in Primary Visual Cortex. *J Neurosci* **28**:12591–12603. doi:10.1523/JNEUROSCI.2929-08.2008

Sun Q-Q, Huguenard JR, Prince DA. 2006. Barrel cortex microcircuits: thalamocortical feedforward inhibition in spiny stellate cells is mediated by a small number of fast-spiking interneurons. *J Neurosci Off J Soc Neurosci* **26**:1219–1230. doi:10.1523/JNEUROSCI.4727-04.2006

Swadlow HA. 2003. Fast-spike Interneurons and Feedforward Inhibition in Awake Sensory Neocortex. *Cereb Cortex* **13**:25–32. doi:10.1093/cercor/13.1.25

Swadlow HA, Gusev AG. 2002. Receptive-field construction in cortical inhibitory interneurons. *Nat Neurosci* **5**:403–404. doi:10.1038/nn847

Swadlow HA, Gusev AG. 2001. The impact of "bursting" thalamic impulses at a neocortical synapse. *Nat Neurosci* **4**:402–408. doi:10.1038/86054

Swadlow HA, Gusev AG, Bezdudnaya T. 2002. Activation of a Cortical Column by a Thalamocortical Impulse. *J Neurosci* **22**:7766–7773. doi:10.1523/JNEUROSCI.22-17-07766.2002

Tremblay R, Lee S, Rudy B. 2016. GABAergic interneurons in the neocortex: From cellular properties to circuits. *Neuron* **91**:260–292. doi:10.1016/j.neuron.2016.06.033

Tsai NY, Wang Fei, Toma K, Yin C, Takatoh J, Pai EL, Wu K, Matcham AC, Yin L, Dang EJ, Marciano DK, Rubenstein JL, Wang Fan, Ullian EM, Duan X. 2022. Trans-Seq maps a selective mammalian retinotectal synapse instructed by Nephronectin. *Nat Neurosci* **25**:659–674. doi:10.1038/s41593-022-01068-8

Usrey WM, Alonso J-M, Reid RC. 2000. Synaptic Interactions between Thalamic Inputs to Simple Cells in Cat Visual Cortex. *J Neurosci* **20**:5461–5467. doi:10.1523/JNEUROSCI.20-14-05461.2000

Usrey WM, Reppas JB, Reid RC. 1999. Specificity and Strength of Retinogeniculate Connections. *J Neurophysiol* **82**:3527–3540. doi:10.1152/jn.1999.82.6.3527

Usrey WM, Reppas JB, Reid RC. 1998. Paired-spike interactions and synaptic efficacy of retinal inputs to the thalamus. *Nature* **395**:384–387. doi:10.1038/26487

Villalobos CA, Wu Q, Lee PH, May PJ, Basso MA. 2018. Parvalbumin and GABA Microcircuits in the Mouse Superior Colliculus. *Front Neural Circuits* **12**:35. doi:10.3389/fncir.2018.00035

Wei P, Liu N, Zhang Z, Liu X, Tang Y, He X, Wu B, Zhou Z, Liu Y, Li J, Zhang Y, Zhou X, Xu L, Chen L, Bi G, Hu X, Xu F, Wang L. 2015. Processing of visually evoked innate fear by a non-canonical thalamic pathway. *Nat Commun* **6**:6756. doi:10.1038/ncomms7756

Whyland KL, Slusarczyk AS, Bickford ME. 2020. GABAergic cell types in the superficial layers of the mouse superior colliculus. *J Comp Neurol* **528**:308–320. doi:10.1002/cne.24754

Wilson JR, Friedlander MJ, Sherman SM. 1984. Fine structural morphology of identified X- and Y-cells in the cat's lateral geniculate nucleus. *Proc R Soc Lond B Biol Sci* **221**:411–436. doi:10.1098/rspb.1984.0042

Zhang Z, Liu W-Y, Diao Y-P, Xu W, Zhong Y-H, Zhang J-Y, Lazarus M, Liu Y-Y, Qu W-M, Huang Z-L. 2019. Superior Colliculus GABAergic Neurons Are Essential for Acute Dark Induction of Wakefulness in Mice. *Curr Biol CB* **29**:637-644.e3. doi:10.1016/j.cub.2018.12.031

Zhao S, Ting JT, Atallah HE, Qiu L, Tan J, Gloss B, Augustine GJ, Deisseroth K, Luo M, Graybiel AM, Feng G. 2011. Cell type–specific channelrhodopsin-2 transgenic mice for optogenetic dissection of neural circuitry function. *Nat Methods* **8**:745–752. doi:10.1038/nmeth.1668

Zingg B, Chou X-L, Zhang Z-G, Mesik L, Liang F, Tao HW, Zhang LI. 2017. AAV-Mediated Anterograde Transsynaptic Tagging: Mapping Corticocollicular Input-Defined Neural Pathways for Defense Behaviors. *Neuron* **93**:33–47. doi:10.1016/j.neuron.2016.11.045

Zucker RS. 1989. Short-term synaptic plasticity. *Annu Rev Neurosci* **12**:13–31. doi:10.1146/annurev.ne.12.030189.000305